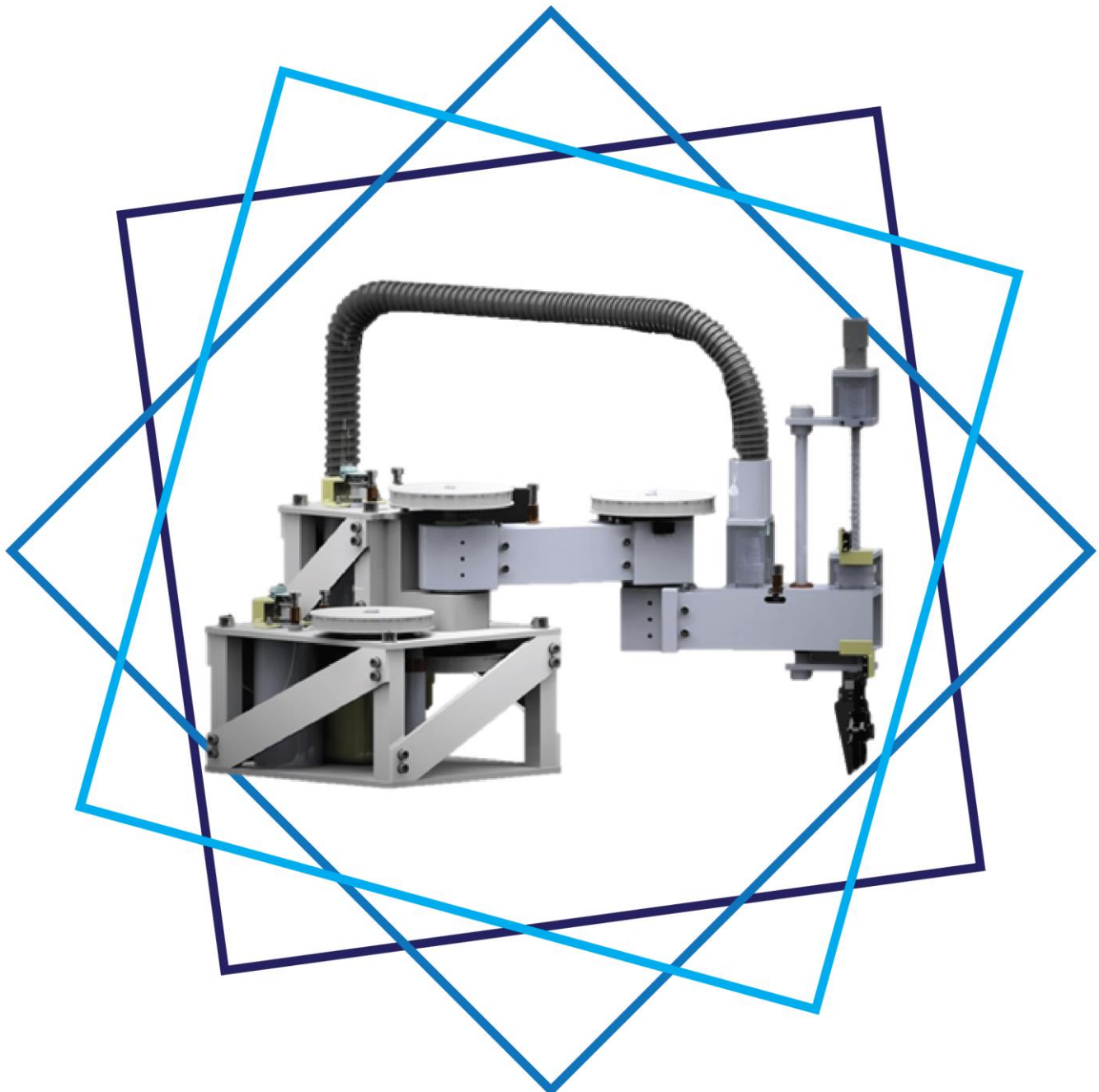


Department of Mechanical Engineering  
Design, Make and Test Final Report

# Robotics Lab



## **Executive Summary**

This report details the design, manufacture, testing and results of a high accuracy, high speed robotic arm used as a lab robot to teach ME4 students robotics fundamentals. The robot to be used in the labs is the £200 Arduino BRACCIO, which our supervisor - Dr. Ristic - thought was too slow and inaccurate, and believed we could design and build a better robot for the same price.

Having undertaken thorough background research of three different robot configurations, a SCARA style robot was deemed the most suitable to satisfy our requirements. Moreover a £30500 industrial robot (the FANUC SR-3iA) was used as our inspiration, with its high speed and high accuracy acting as our performance benchmark.

Following this, the team was split into two groups, a mechanical and an electrical group. The mechanical group worked intensely on design concepts, calculations and produced many CAD iterations until all group members and supervisor were satisfied, with extensive manufacturing then being carried out in the STW. Meanwhile, the electrical group designed all control loops from the ground up, researched and purchased the optimal electrical components and implemented all the software needed to operate the robot.

Unfortunately, due to the outbreak of COVID-19, the robot was not fully assembled, hence key PDS criteria such as speed, accuracy and repeatability were never tested and evaluated. However, simulations were undertaken as part of the extra work package, which indicated that the maximum joint speed was 7.3 rad/s. The robot accelerated to maximum angular velocity in just 0.1 seconds, demonstrating the speed of the robot and satisfying both PDS requirements.

As for the rest of the PDS requirements, the majority were successfully met. The robot had four degrees of freedom, could carry a small 200g payload, had a product life of 4/5 years and could be used safely in the Mechatronics lab using mains power. However, the robot failed our size requirement by taking up a  $35 \times 35 \times 30 \text{ cm}^3$  space as opposed to  $30 \times 30 \times 30 \text{ cm}^3$ , had an operating range between 12.7 cm and 31.2 cm instead of 5cm and 30cm and had a final production price of £455 instead of the specified £200.

In conclusion, despite the failed objectives, the team feels that we successfully delivered a fully programmable educational lab robot with industry standard levels of speed and accuracy, while only spending £522 of the original £1000 budget allocation.

## Contents

<b>Nomenclature</b>	<b>4</b>
<b>1 Introduction</b>	<b>5</b>
1.1 Aims and Objectives . . . . .	5
1.2 Background Research . . . . .	6
1.3 Team Roles . . . . .	9
1.4 Budget . . . . .	10
<b>2 Design Phase</b>	<b>11</b>
2.1 Motor Selection . . . . .	12
2.1.1 Shoulder and Elbow Motor . . . . .	12
2.1.2 End Effector Motors . . . . .	14
2.2 Mechanical Design . . . . .	16
2.2.1 Design Research and Basic Robot Concepts . . . . .	16
2.2.2 Transmission . . . . .	17
2.2.3 Base Structure . . . . .	20
2.2.4 Joints . . . . .	21
2.2.5 Flanges . . . . .	25
2.2.6 End Effector . . . . .	26
2.2.7 Cover and Wiring . . . . .	29
2.3 Electrical Design . . . . .	31
2.3.1 Encoder . . . . .	31
2.3.2 Decoder . . . . .	32
2.3.3 Motor Driver . . . . .	35
2.3.4 Limit Switch . . . . .	36
2.3.5 Arduino Mega 2560 R3 . . . . .	36
2.3.6 Power Supply System . . . . .	38
2.3.7 Graphical User Interface . . . . .	39
2.3.8 Integrated System . . . . .	40
<b>3 Manufacturing Phase</b>	<b>43</b>
3.1 Base . . . . .	44
3.2 Transmission . . . . .	44
3.3 Joints . . . . .	45
3.4 Flanges . . . . .	48
3.5 End Effector . . . . .	49

## CONTENTS

---

3.6 Final Assembly . . . . .	50
<b>4 Testing Phase</b>	<b>51</b>
4.1 Electronics Testing . . . . .	51
4.1.1 Component Verification Tests . . . . .	51
4.1.2 Sampling Frequency Test . . . . .	52
4.2 Integrated Testing . . . . .	52
4.2.1 Repeatability Testing . . . . .	52
4.2.2 Linear Deviation Testing . . . . .	53
4.2.3 Maximum Speed and Acceleration Testing . . . . .	53
4.2.4 Settling Time Testing . . . . .	53
4.2.5 End Effector Speed Testing . . . . .	54
4.2.6 Mass and Storage Dimension Analysis . . . . .	54
<b>5 Impact of Coronavirus</b>	<b>54</b>
5.1 Suspended Activities . . . . .	54
5.1.1 End Effector Assembly . . . . .	55
5.1.2 Full Assembly . . . . .	55
5.1.3 Control System Verification . . . . .	55
5.2 Additional Work Package . . . . .	55
5.2.1 Reflected Inertial Calculations . . . . .	55
5.2.2 Analytical Verification of Electronics . . . . .	57
5.2.3 Control System Simulation in Simulink . . . . .	58
5.2.4 Motion Simulation with Simulink . . . . .	66
<b>6 Discussion and Conclusion</b>	<b>67</b>
6.1 Comparison to PDS . . . . .	67
6.2 Proposal for Continuation . . . . .	70
6.3 Conclusion . . . . .	70
<b>7 Personal Reflective Reviews</b>	<b>71</b>
7.1 Kyriacos Theocharides . . . . .	71
7.2 Aman Didwania . . . . .	72
7.3 Jinhong Wang . . . . .	73
7.4 Advaith Sastry . . . . .	74
7.5 Yikai Wang . . . . .	76
<b>References</b>	<b>78</b>

## Nomenclature

$\alpha$	Lead Screw Angle	$J$	Rotor Interia
$\delta$	Flange Deflection	$J_L$	Inertia of Robot Arm
$\mu$	Coefficient of Friction	$J_R$	Referred Inertia
$\omega$	Angular Velocity	$K_b$	Motor Constant
$\omega_0$	No Load Speed	$K_t$	Torque Constant
$\theta$	Angular Position	$L$	Armature Inductance
$\theta_p$	Graduation Angle of Encoder	$l$	Lead Screw Pitch
$C$	End Condition Coefficient	$L_b$	Length between End Effector Bearing Supports
$CPR$	Counts per Revolution	$L_f$	Maximum Range of Robot
$CPR_t$	Total Counts per Revolution	$N$	Angular Position in Counts
$d_m$	Lead Screw Mean Diameter	$N_i$	Number of counter-clockwise encoder pulses
$d_r$	Root Diameter of the Lead Screw	$N_j$	Number of clockwise encoder pulses
$E$	Young's Modulus	$N_T$	Total Transmission Reduction Ratio
$e$	Motor Back EMF	$N_v$	Critical Speed
$F$	Motor Viscous Damping Factor	$P$	Power
$F$	System Load	$R$	Armature Resistance
$f_p$	Pulse Frequency	$RPM$	Rotations Per Minute
$f_s$	Sampling Frequency	$T$	Torque
$GUI$	Graphical User Interface	$t$	Time
$I$	Mass Moment of Inertia	$T_0$	Stall Torque
$i$	Current	$V$	Voltage
$I_a$	Mass moment of Inertia of arm	$W$	Flange Load
$I_e$	Mass moment of Inertia of end-effector		
$I_l$	Mass moment of Inertia of payload		

## 1 Introduction

### 1.1 Aims and Objectives

In September 2020, the Mechanical Engineering Department will introduce a new course to ME4 students: "Introduction to Robotics". The course aims to teach the fundamentals of robotics via a 'hands-on' approach in the Mechatronics Lab. The Department will use the Arduino BRACCIO as the robot which all the labs will be based on:

Table 1.1: BRACCIO specifications

Specification	Value
Price	£200
Weight	792 g
Max Range	80 cm
Max height	52 cm
Max load	150 g
Operating angle	180 °
Voltage supply	4.8 V OR 6 V
Max current	4 A
Motor angular velocity	0.36 sec/180 °

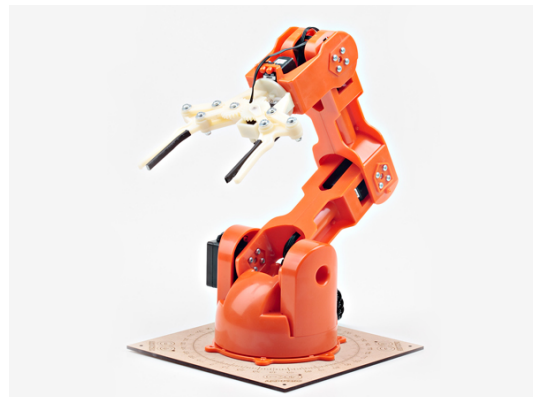


Figure 1.1: Arduino BRACCIO

The BRACCIO contains 21 plastic components to be assembled. It is programmable in the Arduino environment, hence requires an Arduino board which must be purchased separately. Furthermore, the device utilises six servo motors connected by a direct drive to power the joints.

As a teaching tool, the BRACCIO is notably sub-par. The low-quality materials, crude fastening methods and backlash of servo motors result in large positional errors. Moreover, the cheap low powered servo motors provide slow, jittery motion when a load is being carried at full extension. The educational potential of the BRACCIO is limited as the control loop hardware is inaccessible for students. This prevents experimentation and comprehension of implementing control in robotics. Overall, the Department requires a faster, more accurate and modular robot to enhance the learning experience of students. Limitations include a low budget of approximately £200.

The drawbacks were discussed with the project supervisor in the initial meeting. Both parties agreed that the BRACCIO is unsuitable as an educational tool. The purpose of the DMT was to design a more capable robot. The following outlines were devised to indicate expected robot performance.

1. Readily reproducible

2. Control loop must be fully modular
3. Designed to perform simple pick and place and low load tasks
4. Faster and more accurate than the Arduino BRACCIO
5. At least four degrees of freedom
6. Easily stored within the CAGB building
7. Rival the BRACCIO in price

## 1.2 Background Research

With defined rough guidelines for our project, research on existing robot products was carried out to determine which configuration would be best suited for the application. Different types of robots investigated include:

- **SCARA** (Selective Compliance Assembly Robot Arm) robot [1] (e.g Fanuc SCARA series [2])
- **Articulated Robots** [3] (e.g. Braccio Robot by Arduino [4], robot developed by Elfasakhany et al.[5] and experimental teaching robot [6])
- **Cartesian Robots** [7] (e.g. gantry robot [8]). Fig. 1.2 shows the typical structure of each robot type and comparisons can be found online [9].

A morphological analysis based on the literature review (Table 1.3) was conducted on key factors such as accuracy, speed, working space, structural robustness and weight. Table 1.2 summarises the conclusions on the suitability of each robot configuration.

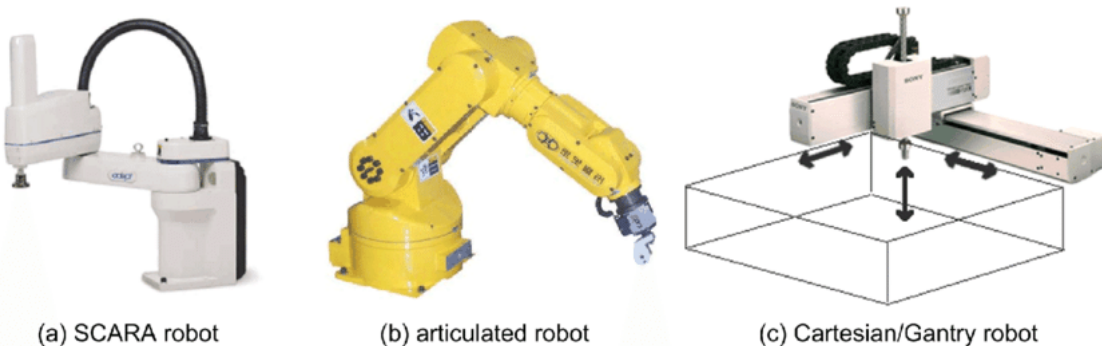


Figure 1.2: Different Types of Robots Researched [9]

Table 1.2: Conclusions on Robotic Configurations

SCARA	<p>Based on our research and morphological analysis, SCARA came out as the most suitable configuration for this project. The main advantage was that the flanges operate in a horizontal plane as opposed to vertical. As such, the load is carried in the joints and not the motor. This results in a fast and accurate response, as the motor only deals with the inertia of the arm and does not need to counteract gravitational forces. Moreover, a SCARA robot has a large working space given its size [2] and can be compactly stored. Provided that the joints and flanges are stiff, a SCARA configuration is robust and will be able to withstand hours of use in the lab.</p> <p>One disadvantage of the SCARA configuration is the end effector mechanism is more complex than an articulated configuration, requiring inverse kinematics calculations to correctly position the end effector [1]. Another disadvantage is that there is a minimum of two links. Hence errors in the first link are amplified by the second [10]. The majority of robots used in industry 'pick and place' operations such as factories are SCARA robots [2].</p>
Articulated	<p>The Articulated configuration was deemed to be the least suitable following the review, with no clear advantages over the SCARA or Cartesian configuration, other than a simpler end effector mechanism. As mentioned earlier, the motors powering the joints of the Articulated robot have to drive the inertia of the flanges and counteract the gravitational forces, (which inhibits speed and accuracy) and were often found to be placed on the joints themselves rather than on the main body[4], [6], thereby increasing the inertia of the arms. Moreover, the working space is inferior to Cartesian configurations if servo motors are used as these have limited rotational capabilities [5] whereas the storage size is roughly equivalent to SCARA.</p> <p>Generally, articulated robots exhibit inferior performance to both SCARA and Cartesian with no size, weight or price advantage over SCARA, unless a parallelogram configuration is used which is proven to be stiffer than equivalent SCARA configurations [11]. However, for the purposes of our project a parallelogram design is far too complex.</p>
Cartesian	<p>This configuration showed clear advantages over the other two when it came to working space. Moreover, Cartesian robots can perform pick and place tasks with very high accuracy [7] as errors are not amplified by any links (aka "joints") but are generally slower than either SCARA or Cartesian configurations [1]. Furthermore, the Cartesian robot is less complex than either the SCARA or Articulated configurations as it doesn't need inverse kinematics calculations to correctly position the end effector mechanism [1].</p> <p>The main disadvantages of the Cartesian configuration however is its storage size and weight. Given the time constraints of the project as well as the need to be easily stored, it was decided that the Cartesian configuration would not be suitable for our application despite some key advantages over both SCARA and Articulated configurations.</p>

Table 1.3: Morphological chart of the three configurations. '1' is the least desirable score and '5' is the most

	SCARA	Articulated	Cartesian
Size	3	3	2
Working Space	4	3	5
Weight	3	2	1
Complexity	3	3	4
Speed	4	3	2
Accuracy	4	2	5
Repeatability	4	3	5
Robustness	3	2	3
Price	3	3	2
Total	31	24	30

Towards the beginning of our literature review, the project supervisor had suggested that a SCARA robot may be the most suitable configuration, which was verified with the findings of our research. Moreover, having researched SCARA robots in-depth, a suitable robot was discovered which would serve as the inspiration for our design and expected performance: the "FANUC SR-3iA" [12]. The robot provided a benchmark for the development of our PDS in the design phase of the project.

Table 1.4: FANUC SR-3iA specifications [12]

Specification	Value
Price	£30500
Weight	19kg
Max Range	40cm
Max height	15cm
Max load	3kg
Operating angle	360°
Repeatability	0.01mm
Voltage supply	200-230V
Max current	10A
Motor angular velocity	0.06 sec / 180°



Figure 1.3: FANUC SR-3iA [12]

### 1.3 Team Roles

Table 1.5: Team Member Roles and Responsibilities

Team Member	Role(s)	Responsibilities
Kyriacos Theocharides	Project Manager Mechanical Team Member	Updates Gantt chart, checks progress and sets deadlines. Checks with other team members to see if the quality and speed of work is satisfactory. Arranges meetings within the group or with supervisors included and ensures that there is clear communication within the team. Assists in design, manufacture and testing of mechanical components.
Aman Didwania	Inventory & Budget Manager Electronics Team Member	Must keep track of budget and inform project manager if team is drastically overshooting or undershooting budget expectations. In charge of order and delivery of components. Joint responsibility of designing the control system with Advaith.
Jinhong Wang	Research, Design & Test Manager Mechanical Team Member	Responsible for conceptual and embodiment design phase. Researches at every step of ways to improve the project design. Responsible for SOLIDWORKS and SIMULINK processes. Approves testing methods, benchmarks, results and evaluation of results. Oversees any change in design.
Advaith Sastry	Document & Data Manager Electronics Team Member	Responsible for monitoring and quality control of project documentation. Must keep a copy of every iteration of documentation complete with number and date. Ensures documentation deadlines are met. Joint responsibility of designing the control system with Aman. Responsible for additive manufacturing
Yikai Wang	Manufacturing & Assembly Manager Mechanical Team Member	Ensures manufactured components are of the required quality. Investigates whether design is feasible and what materials are required. Communicates with STW and Hackspace managers. Ensures that manufacturing is happening on schedule according to Gantt chart. Responsible for quality of engineering drawings. Responsible for assembly and programming of prototypes.

## 1.4 Budget

A total budget of £1000 was allocated by the Department of Mechanical Engineering for this Design, Make and Test Project. The project did not have any additional funding. Fig. 1.4 provides a breakdown of expenditure:

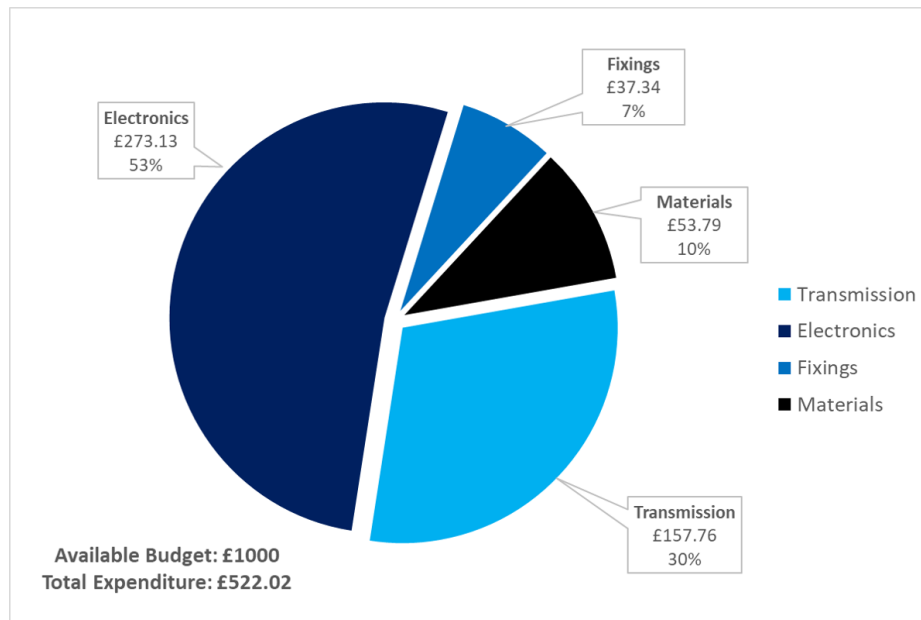


Figure 1.4: Breakdown of Expenditure

The expenditure associated with the project was significantly under-budget. This was as expected, as one of the key objectives was to optimise costs to be competitive with the current robotic manipulator planned for usage in the ME4 Introduction to Robotics Module - the Arduino BRACCIO.

Only one set of electronic components were ordered for testing; in order to make room for changes, it was planned that the remainder of the electronics would be purchased after testing. However, due to COVID-19, the stage was not reached, resulting in the remaining components not being purchased. Therefore, this expense is not reflected in the total expenditure.

Consequently, although Fig 1.4 shows an expenditure of only £522, the cost price of the robot (incorporating the unordered components), without available bulk purchasing discounts, amounts to roughly £640.

## 2 Design Phase

Based on the background research conducted and customer requirements, the final product design specification is shown in Table 2.1.

Table 2.1: Final Product Design Specification

Objective	Criteria	Verification
Weight	Total weight must be under 4 kg.	
Size	Fit a $30 \times 30 \times 30 \text{ cm}^3$ space.	
Payload Properties	Max payload of 200 g. Max dimensions: 10 cm x 5 cm x 2 cm. Min dimensions: 1 cm x 0.5 cm x 0.5 cm	Testing
Degrees of Freedom	Four Degrees of Freedom.	
Operating Angle	180 degrees	Design Review
Operating Distance	Radius between 5 and 30 cm.	Ruler - Testing
Accuracy	Difference between actual and simulated positions - $\pm 0.01 \text{ mm}$ linear deviation.	
Repeatability	Less than $\pm 0.1 \text{ mm}$ error for repeated position.	
Settling Time	The time taken for the arm to stabilise after reaching intended position - 0.1 s max.	
Max Speed	At least $2\pi \text{ rad/s}$	
End Effector Speed	150 mm vertical distance in at least 1.5 seconds	
Acceleration	Reach max angular velocity in less than 0.2 seconds.	
Environment	Product is expected to operate in indoor conditions 20-30 °C, no/low humidity. May be exposed to dust and debris (IP62). Critical transmission parts with IP65 (dustproof when storing).	
Product Life	Expected shelf life of 4/5 years.	Design Review
Service Life	3 hours of lab session every week, 35 weeks a year (315 hours total)	Simulation & Fatigue Calculation
Repairability	Mechanical components must be easily replaceable.	
Manufacturing	Easily reproducible.	
Product Cost	Price per unit must be lower than BRACCIO price, at the most approximately £200 per unit.	Design Review
Safety	No sharp edges. No exposed transmission or electrical components.	Testing & Design Review
Disposal	Components (except motors/electronics) must be recyclable.	Design Review

## 2.1 Motor Selection

For motor selection, stepper motors and servo motors were initially investigated. Stepper motors work on principles of open-loop control. The utilisation of steppers made achieving the accuracy stated in the specifications unrealistic while subtracting from the educational aspects of the robot. Programming a closed-loop system is significantly more complicated, allowing for a greater variety of practical work relative to an open-loop system.

Servo motors were disregarded due to budget constraints. Additionally, servos do not allow students to interact with the position feedback mechanism. To provide a closed-loop system which does not exceed the allocated budget, the conclusion was drawn to design the control system around a simple DC motor.

### 2.1.1 Shoulder and Elbow Motor

As the aim of the project was to design a fast powerful robot, a motor that exceeds requirements was selected. Reduction of the power supplied by an over-powered motor is easier and more cost-effective than replacing an under-powered motor. An estimate of the required power was determined using Eq. 2.1-2.2.

$$I \frac{d^2\theta}{dt^2} = T_0 - \frac{T_0}{\omega_0} \frac{d\theta}{dt} \quad (2.1)$$

$$P = \frac{T_0 \omega_0}{4} \quad (2.2)$$

Where  $I$  is the mass moment of the inertia,  $\theta$  is the angular position,  $T_0$  is the stall torque of the motor,  $\omega_0$  is the no-load speed and  $P$  is the power of the motor.  $\omega_0$  was taken as  $2\pi$  rad/s as per the PDS, and mass moment of inertia was estimated as follows:

$$I = I_l + I_a + I_e \quad (2.3)$$

Where  $I_l$  is the mass moment of inertia of the payload,  $I_a$  is the mass moment of inertia of the arm and  $I_e$  is the mass moment of inertia of the end-effector.

Table 2.2: Mass Moment of Inertia Calculation

$I_l$	$I_a$	$I_e$	$\Sigma I$
0.05	1.125	0.25	1.425 kgm <sup>2</sup>

Fig. 2.1 shows the position-time relationship using the values above at different motor stall torques.

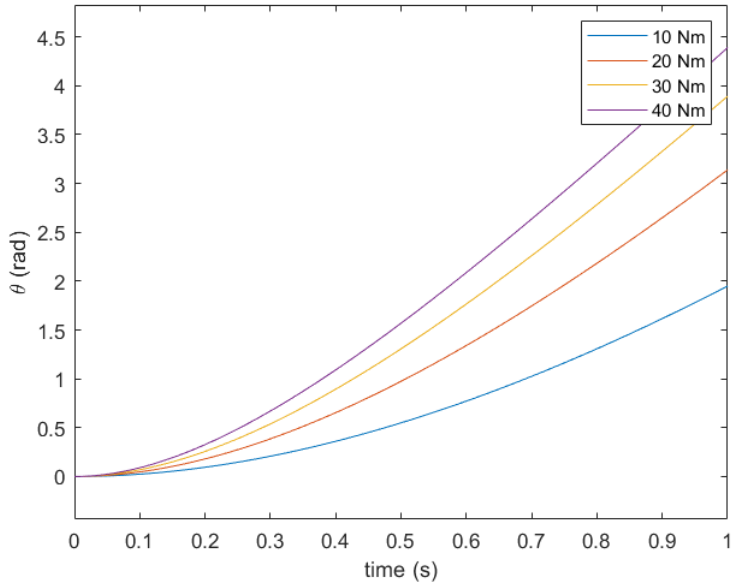


Figure 2.1: Graph of Angular Position against Time for different values of Stall Torque

The time to complete a full sweep of the robots range ( $\pi$  radians) should be less than 1 second. Hence, the stall torque was required to be greater than 20 Nm. Minimum power (as per Eq. 2.2) would be  $10\pi$  which is approximately 30 W. Due to the accuracy requirement, a pulley transmission was preferable to gears (see Section 2.2.2). The disadvantage of pulleys, however, is the difficulty in achieving high transmission ratios - the greater the difference in the diameter of two pulleys, the number of teeth in contact on the small pullet is reduced, thus reducing transmission efficiency. Therefore, a motor with high torque and low no-load speed would be preferred so that a lower transmission ratio would be required.

Table 2.3: Operation Parameters of Motor

Parameter	Value
Rated Voltage	24 V
Rated Current	3 A
Power Output	80 W
Weight	1.35 kg
Stall Torque	1.22 Nm
No-Load Speed	2500 RPM
Motor constant	0.09 Vsrad <sup>-1</sup>



Figure 2.2: Elbow/Shoulder Motor

The last factor that affected motor selection was budget; considering the price of the robot should

be under £200 (as per specification), utilising significant proportions of the overall budget was undesirable. With consideration of the aforementioned factors, the motor in Fig. 2.3, costing of approximately £15, was chosen. Fig. 2.3 shows the motor graph. Table 2.3 details the motor's operating parameters.

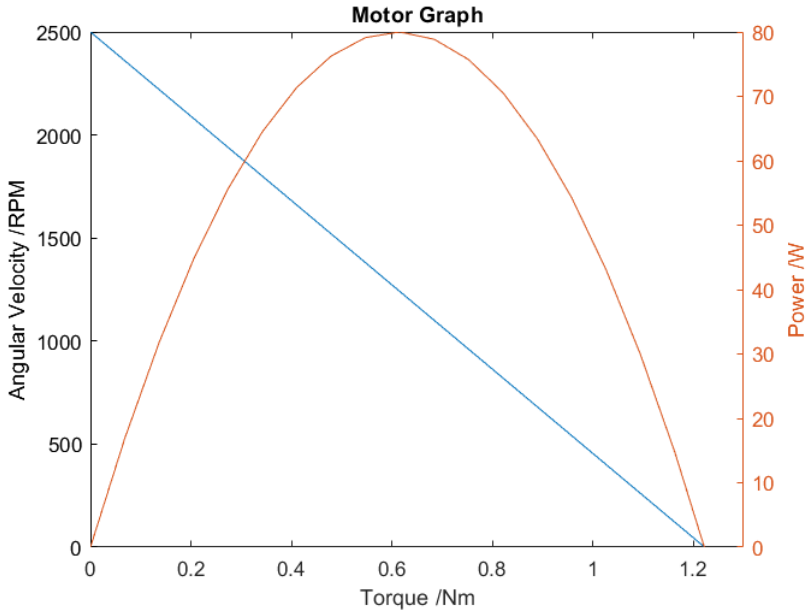


Figure 2.3: Motor Characteristics

### 2.1.2 End Effector Motors

The torque required to drive the ACME lead screw was determined using Eq 2.4. The parameters for the calculation of the required torque is shown in 2.4[13].

$$T_{raise} = \frac{Fd_m}{2} \left( \frac{l + \pi\mu d_m \sec \alpha}{\pi d_m - \mu l \sec \alpha} \right) \quad (2.4)$$

Where  $T_{raise}$  is the raising torque,  $F$  is the applied load,  $d_m$  is the mean diameter,  $\mu$  is the coefficient of friction,  $l$  is lead screw pitch and  $\alpha$  is the lead screw angle.

Table 2.4: Raising Torque Calculation Parameters and Values

$T_{raise}$	$F$	$d_m$	$\mu$	$l$	$\alpha$
0.0099	1 kg	8 mm	0.15	2 mm	29°
0.0199	2 kg	8 mm	0.15	2 mm	29°

With the moving parts and an approximate load of 0.2 kg, the total combined weight of the end effector and payload was between 1.2 ~ 1.6 kg, hence a motor with 0.01 ~ 0.02 Nm torque is

required. To achieve PDS specifications, 150 mm of vertical distance must be covered within 1.5 seconds. The required speed in RPM was calculated using Eq. 2.5.

$$\text{Speed} = \frac{150 \div 1.5}{l} \times 60 = 3000 \text{ RPM} \quad (2.5)$$

DMN37BA was selected for vertical motion as the motor provides a torque of 0.014 Nm and speed of 4700 RPM. Employing a transmission ratio of 2 : 3 produces 0.021 Nm and 3133 RPM satisfying the PDS. GA20-N20 was the selected motor for the rotation of the end effector and it required the same torque but lower speed, as the requirement for rotation was 180° in 1s. Hence a 12 V 30 RPM motor which generates a torque of 0.03 Nm was chosen. The motor specifications for the end effector are given in Table 2.5.

Table 2.5: Operation Parameters of DMN37BA[14] and GA12-N20[15]

DMN37BA		GA12-N20	
Parameter	Value	Parameter	Value
Rated Voltage	12 V	Rated Voltage	6 V
Rated Current	1.01 A	Rated Current	0.15 A
Power Output	7.2 W	Power Output	3 W
Weight	0.8 kg	Weight	0.022 kg
Rated Torque	0.014 Nm	Rated Torque	0.03 Nm
Rated Speed	4700 RPM	Rated Speed	30 RPM

Further analysis was conducted to ensure the shaft does not operate at 80% of the critical speed. This analysis was conducted to avoid vibration-induced whirling. Eq. 2.6 was used to evaluate the critical speeds and results are shown in Table 2.6 [16].

$$N_v = \frac{(4.76 \times 10^6) d_r C}{L_b^2} \quad (2.6)$$

Where  $N_v$  is the critical speed in RPM,  $d_r$  is the root diameter of the lead screw,  $C$  is the coefficient for the end condition and  $L_b$  is the length between bearing supports.

Table 2.6: Critical Speed Calculation Parameters and Values

$0.8N_v$	$d_r$	$C$	$L_b$
125240 RPM	8 mm	0.37	300 mm
70448 RPM	8 mm	0.37	400 mm

This concludes running at 3000 RPM is well below critical speed.

## 2.2 Mechanical Design

In this section, the mechanical design process of the project is explained. The final mechanical design is shown in Fig. 2.4. For clarity, the main project is divided into sub-assemblies and discussed in detail in the following subsections.

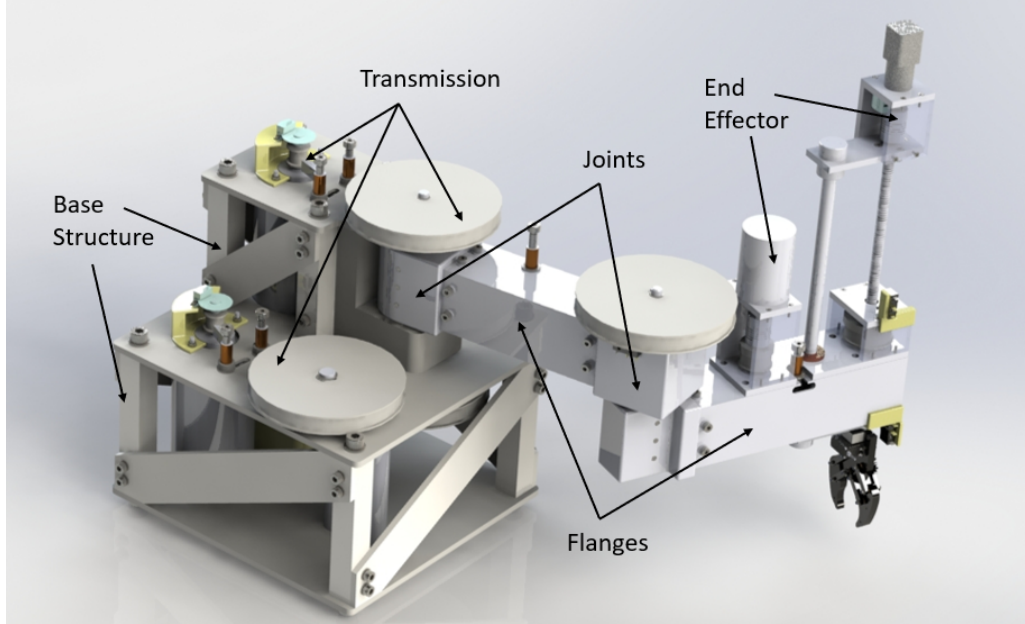


Figure 2.4: Final Prototype Mechanical Design of the Robot

### 2.2.1 Design Research and Basic Robot Concepts

To fulfil the four degrees of freedom design requirement, a simple illustration of the design is shown in Fig. 2.5. As shown, there are two horizontal flanges and an end effector with two degrees of freedom (linear degree of freedom along the z-axis and rotational degree of freedom around the z-axis). The detailed design to achieve this is further explained in Section 2.2.2 and 2.2.6.

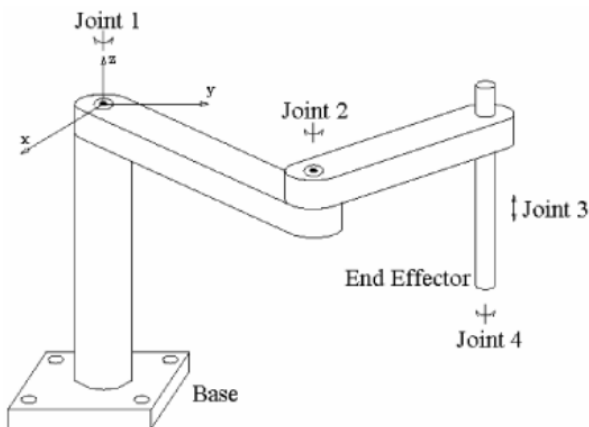


Figure 2.5: Basic SCARA configuration [17]

### 2.2.2 Transmission

With the motor selected in Section 2.1.1 it was difficult to have a direct-drive transmission because of the high-speed low torque characteristics. Additionally, it was impractical to have a built-in motor at the elbow joint due to its size and weight. After calculation, to achieve the speed of  $2\pi$  rad/s specified in the PDS, a two-stage reduction with a maximum total reduction ratio of approximately forty-two was required.

Table 2.7: Evaluations of transmission concepts

Transmission Type	Advantages	Disadvantages
Gears	High gear ratios Simple Structure	Large backlashes
Hydraulic Actuators	Trivial backlashes	High tolerances Expensive costs
Belts	Low backlashes	Complicated belt route design
Chains	Low backlashes	Complicated chain route design Heavy

Multiple transmission concepts were compared including gears, belts, chains, and hydraulic actuators. Minimising backlash was the top priority when designing the transmission system. Although gears can employ large transmission ratios (up to seventy-two for worm gears), the resulting backlash was significant. As a two-stage transmission is required and the joints for the shoulder and elbow were serially connected, even small backlashes between each gear mesh would lead to large inaccuracies at the end effector. As an alternative design, anti-backlash gears reduce the problem, but the high costs and maintenance difficulty made them unsuitable for the project.

Hydraulic actuation [11] has trivial backlashes, but the high tolerances in manufacturing and calculations meant that the budget of the project was insufficient. Flexible transmissions, such as chains and belts, were good solutions for low backlash. Additionally, the concept depicted in Fig. 2.5 requires long-range transmissions (across the length of the proximal flange), which supports the selection of flexible transmission systems over rigid. Moreover, belt transmission is generally lighter than chain systems hence timing belts and pulleys were selected over other types of transmissions.

Based on timing belt selection procedures [18], the application was considered to have soft starts, be light-duty and have a design power that required a module of five. The minimum and maximum teeth sizes available in the catalogue were twelve and seventy-two. This lead to a 1:6 gear ratio for each reduction stage. For manufacturing simplicity, both stages were designed to

have the same reduction ratio, leading to a total ratio of 1:36. The motor selected in Section 2.1.1 operates at 2500 RPM. The resulting speed of joints was approximately 69.4 RPM which satisfies the PDF requirements.

As mentioned, the motors selected are too heavy and large to fit onto the elbow joint. Hence the transmission was designed to originate from the fixed robot base. As the elbow joint is free to move, the position on the base must be a constant distance to the elbow joint during operation. The only suitable position was on the shoulder shaft (Joint 1 in Fig. 2.5). This is because the distance was always the length of the proximal flange.

Ideally, an additional transmission shaft was required on the same axis of the shoulder shaft, to link the motor and the elbow joint. However, this leads to high tolerances in alignments of the shafts, causing additional complexity in manufacturing. A simpler solution was proposed as shown in Fig. 2.6, where two pulleys were connected face to face with a bush bearing inserted in the centre. The assembly of pulleys functions as an intermediate shaft on the shoulder shaft, with independent rotation. This design eliminates the concentricity problem with two separating shafts while ensuring the control of the elbow joint is independent of the shoulder joint position.

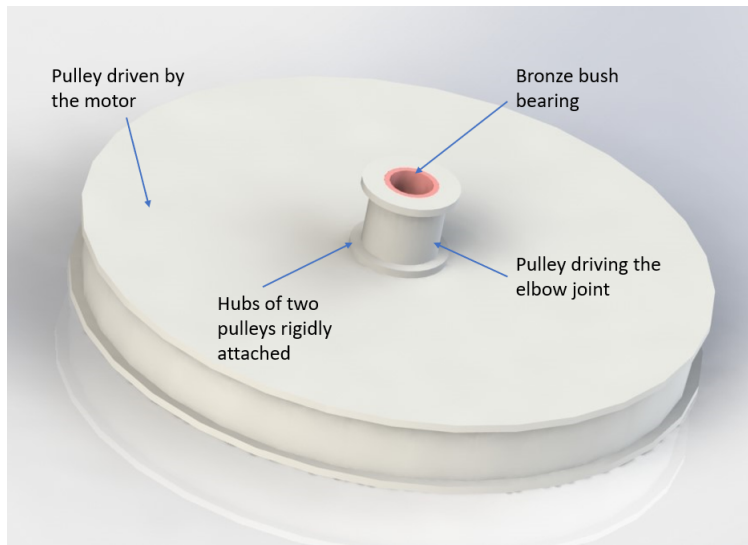


Figure 2.6: Concept of Reduction Pulleys

After deciding the transmission methods and elements, the transmission layout was determined. During the design phase, many different arrangements of the motors, intermediate shafts and pulleys were proposed. The final design, which is shown in Fig. 2.7, was selected after several iterations. This design provides a compact arrangement of the transmission elements, mostly close to the mounting plate or the neighbouring components. The layout reduces the size of the final products and also reduces the bending moment on the shafts due to tension from the belts. For

both the intermediate shaft and the shoulder shaft, two bearings are supported by the same bearing housing, eliminating alignment issues in manufacturing. The mounting plates could be laser-cut for accurate hole positions (hence shaft positions). The tolerances for aligning mounting plates are not critical for the transmission system. Although the motor driving the elbow joint was overhanging above the base, space underneath was utilised for the electronic component box (yellow block shown in Fig. 2.7) therefore both the motors were supported by the base.

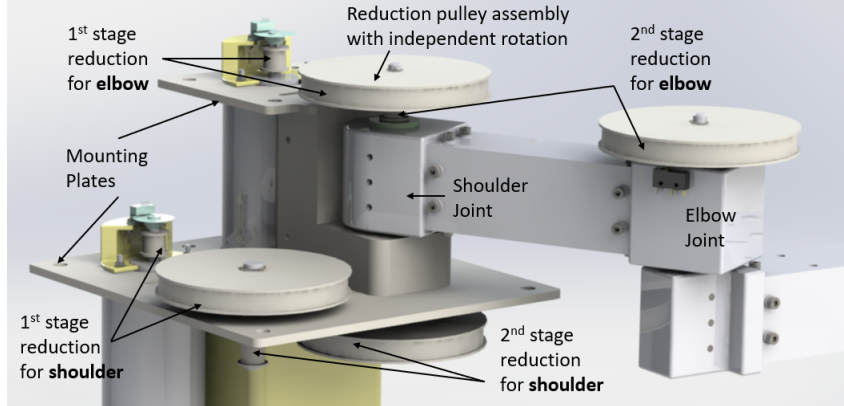


Figure 2.7: Final Transmission Layout of the Shoulder and Elbow joints

As a flexible transmission was selected for this project, tensioners were required. Loosening of the belts during operations may lead to slip in the timing belts, which undermines the performance of the robot. Traditionally, an idler is fit on the slack side of the belt. However, two idlers were required for each reduction stage because the motors drive in both clockwise and anti-clockwise directions. There are four transmission stages in total, hence eight idlers for the shoulder and elbow transmission were required.

Instead of manufacturing eight idler shafts, shoulder bolts (shown in Fig. 2.8) were selected as substitutes because of standardised tolerances and fixtures to the mounting plate. Bronze bush bearings were assembled with the shoulder bolts to act as idlers. Appropriate nylon spacers would raise the idlers to the ideal height. Nuts were tightened on the other side of the plate to fix the idler positions. Furthermore, one of the idler shaft's position can be adjusted to tighten the belts in case of loosening. [19]

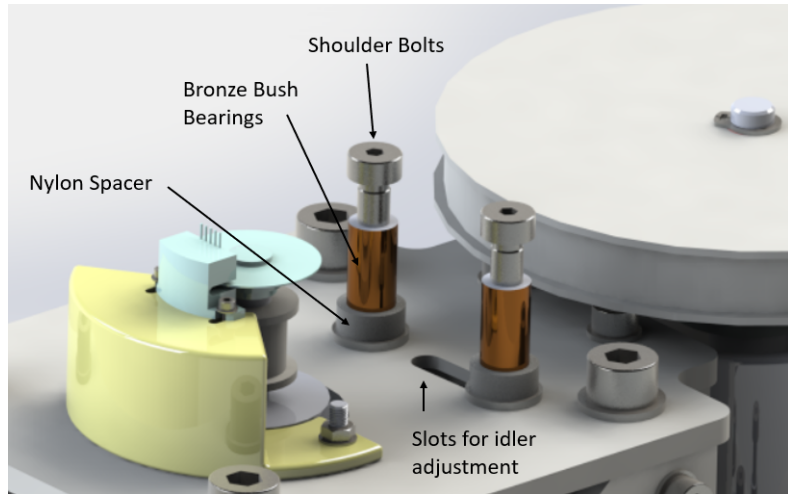


Figure 2.8: Shoulder Bolt Idler Design

### 2.2.3 Base Structure

After the transmission layout was finalised, the supports for the structure and transmission elements were developed. With consultation from technicians and metal suppliers, three options were available for the project.

Firstly, the mounting plates could be simply supported by four metal pillars bolted at the corner for a rectangular frame. This solution provided vertical support to the structure, but could not withstand large torques from the shafts. Hence if large shear stresses are applied, relative rotations may occur between different mounting plates.

The second option was to buy a large box section of steel and machine off the top to have a deep U shaped bracket as the base. This provides high stiffness in both directions, with sealed walls on the two sides. However, the price for suitable box section beams cost more than £700 hence is completely out of the budget of the project.

Finally, a combination of both concepts (a space frame design) shown in Fig. 2.9, was selected for this robot. Between the two mounting plates, four square aluminium bars with 20 mm side lengths were bolted to each corner using M8 cap screws, as suggested in option one. Additionally, to withstand large torsional stresses, laser-cut side plates were bolted to the pillars on the side. Additional support was provided by the shoulder support and the idler supports to enhance the structure. A space frame that is stiff in all directions was hence built for the robot. The dimensions for the base plate was 220 x 240 mm which is less than the specified storage dimensions.

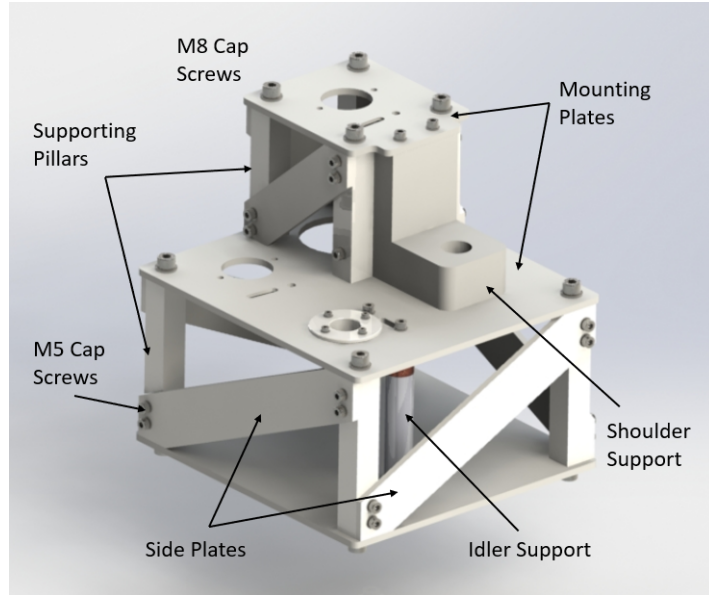


Figure 2.9: Base Design of the Robot

#### 2.2.4 Joints

Another important aspect of the design was the shoulder and elbow joints, and their respective supports.

**Shoulder joint:** Since the whole flange/end effector assembly is a cantilevered structure, the shoulder joint support experiences the most load in the robot. Similarly, the shoulder shaft experiences the largest bending moment. The shaft design for the shoulder joint was one of the most important aspects that would contribute to the success of the project as a whole.

Several iterations of shoulder joint design occurred. To take the load, the bearings should be well separated to minimise the bending moment induced stress. Three concepts were shown in Fig. 2.10 with red arrows annotating the bearing separation in the design..

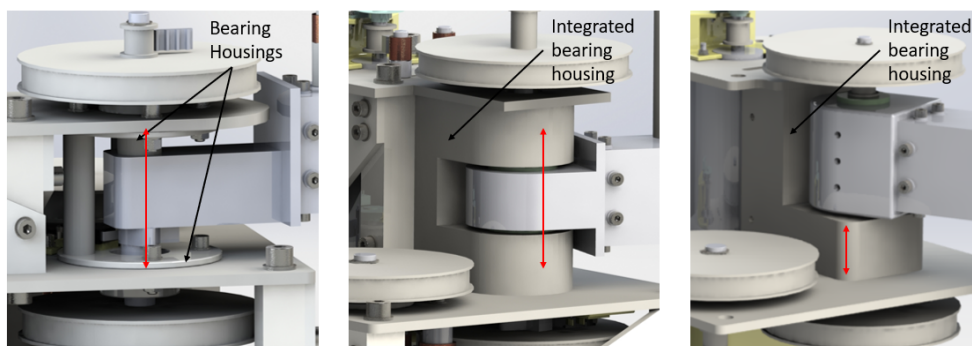


Figure 2.10: Three shoulder joint support concepts: **Left:** bearing housing design, **Middle:** integrated support design, and **Right:** improved integrated support design

The first option was to have separate bearing housings on the top and mid mounting plate, shown on the left of Fig. 2.10. This provides sufficient bearing separations and minimises the shoulder shaft length. However, the design is highly dependent on the concentricity of the bearing housing holes when manufacturing and the thin plates may deform during operation.

The second option was to have an integrated shoulder support with bearings on both side of the shoulder joint, as shown in the middle of Fig. 2.10. The integrated bearing housing provides rigid joint support from one piece of material. However, it still depends on the concentricity when machining the holes and it is practically hard to restrain the bearings on the shoulder shaft and to assemble the shoulder joints.

Therefore, an improved integrated shoulder support design is shown on the right of Fig. 2.10. Although the bearing separation has decreased compared to the other two concepts, placing both bearings on one side of the shoulder joint will solve the problem of concentricity in the other concepts. In addition, belt tension from the top will balance the bending moment from the flange/end effector assembly, hence minimising the effect of reduced bearing separation. A detailed view of the final shoulder support design is shown in Fig. 2.11.

The component that connects the shoulder shaft and the flanges is the shoulder connector. It is a rigid block of aluminium that is bolted to the flanges (which will be further introduced in Section 2.2.5). During operation, the joint will rotate with the shoulder shaft and hence perform the actuation of the shoulder degree of freedom.

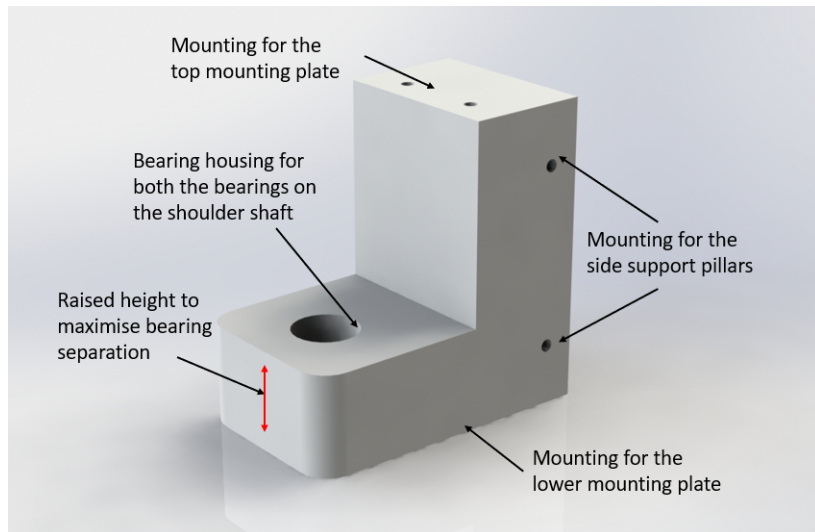


Figure 2.11: Final Design of the Shoulder Joint support

For the assembly of the shoulder joint, a compact shaft design is shown in Fig. 2.12. The shoulder joint was mounted to the shaft with dowel pins. Teflon washers were added to reduce the friction

between the rotating joints and the mounting plates. The distance between the two bearings was set by an external spacer. A cam was specifically designed for the shoulder joint to activate the limit switches when the joint reaches maximum limits. The limit switches will be further introduced in Section 2.3.4. Both the cam and pulley driving the shoulder shaft were fixed by a 4 x 4 steel key.

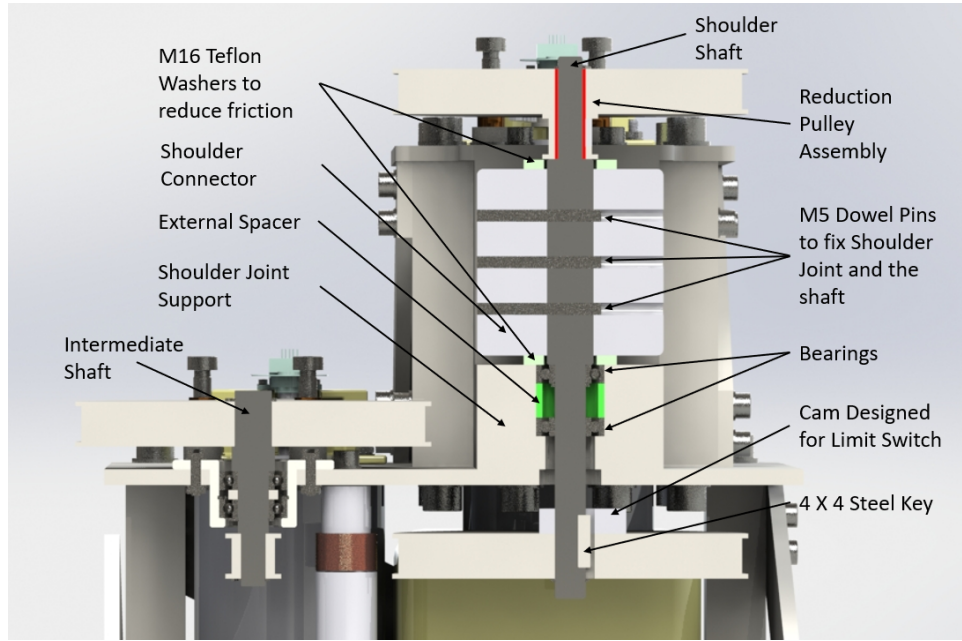


Figure 2.12: Shoulder Shaft design details

### Elbow joint:

The elbow joint is also a key component that heavily influences the performance of the robot. This is specifically important in SCARA robots as joints must be designed to rotate with little friction and withstand the load of the flanges, end effector mechanism and load without bending. An effective elbow joint is light without sacrificing stiffness. Leading up to the final design of the elbow joint, three iterations were considered and ultimately rejected as displayed in Fig. 2.13 below:

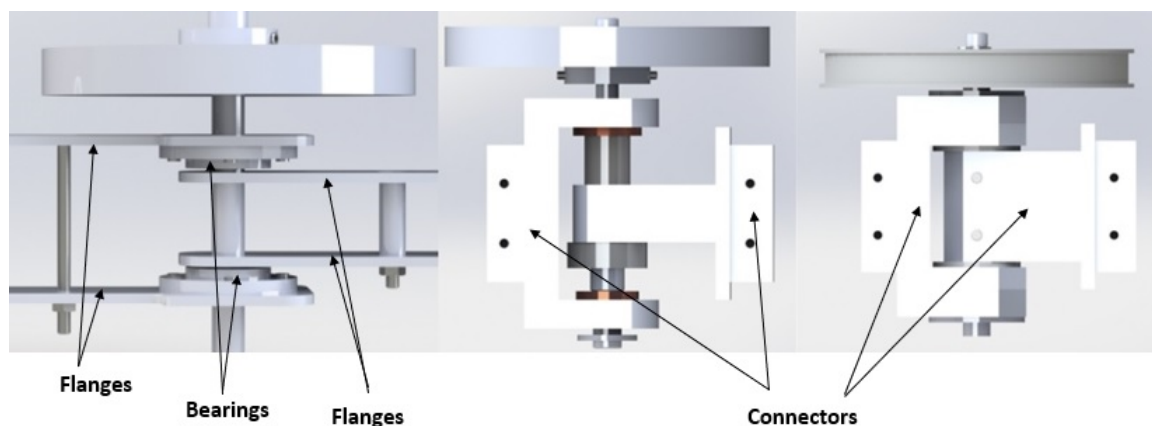


Figure 2.13: Three elbow joint iterations: **Left:** 1st Design, **Centre:** 2nd Design, **Right:** 3rd Design

The first design attached the flanges directly to the bearing housing with small bolts and to the shaft with glue. This design focused on ease of manufacturing, keeping the number of components low and simple to make. The flanges would have been laser cut and bolted together. However, the design was rejected as the flanges were thin and the bolts were inadequate to support the load of the structure, thus enabling large deflections.

The second design incorporated connectors machined out of an aluminium block that attached on to the flanges via M4 bolts. This design increased stiffness. The design was also disassemblable, making use of a shaft collar and spacer to constrain the inner connector. Bush bearings were favoured over ball bearings to save space. However, the added penalty was greater friction during elbow operation. The major flaw in this design was the wasted space between the connectors used for the shaft collar and spacer.

The third design omitted the spacer and shaft collar, instead attaching the inner connector to the shaft via dowel pins. Also, the bearing housings were milled into the outer connector itself, saving space and allowing ball bearings to be used instead of oilite bush bearings. Overall this design was an improvement in many aspects. The drawback was that once assembled it could not be disassembled, due to the dowel pins constraining the inner connector. Finally, the connectors could be made larger to further increase stiffness.

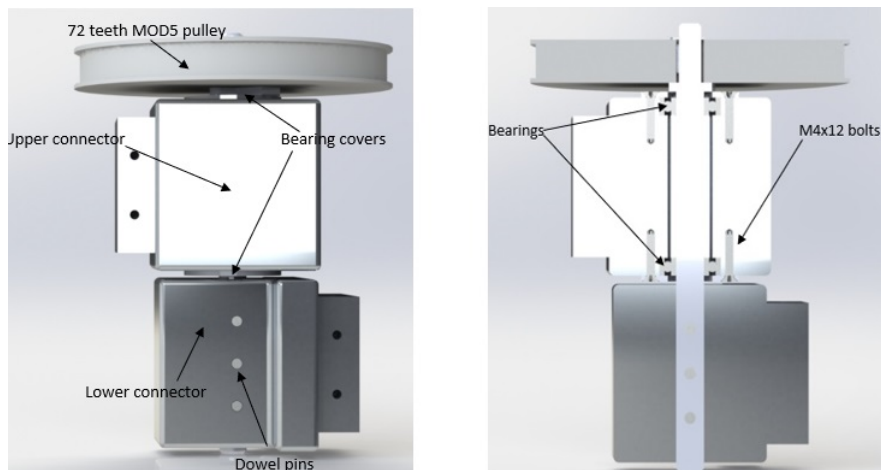


Figure 2.14: Final elbow joint design: **Left:** Elbow connector, **Right:** Cross section view

The final elbow design consisted of an upper-lower connector configuration with the pulley mounted at the top of the shaft (Fig. 2.14). The key reasons why this design was selected are highlighted in Table 2.8:

Table 2.8: Justification for Final Elbow Flange Design

Justification for Elbow Design
An upper-lower connector configuration was chosen as this allowed the size of the connectors to be increased. Bigger connectors are stiffer and therefore deflections and bending are minimised at the joint.
An upper-lower configuration allowed greater rotation than an inner-outer configuration (as was the case in the previous 3 designs), thereby increasing the robot's working envelope.
The bearing housings were integrated into the connectors, reducing manufacturing time and keeping the design compact. The bearings were constrained by the bearing covers which are bolted into the connectors.
The lower connector is constrained by three dowel pins to the shaft so there is no slip even at high speed/torque movements while still allowing partial disassembly of the joint.
All materials and components (other than bearings and pulley), were available from ME Stores and were manufacturable with equipment in the STW.

The disadvantages of this design were that it is heavier than previous iterations due to the size of connectors. Manufacturing was also trickier due to the strict tolerances of the bearing housing. Finally, the shaft was longer and subject to increased bending moments. Further analysis with MATLAB showed that this difference is negligible. As mentioned previously, stiffness and strength of joints were of paramount importance in the robot's design. These disadvantages are acceptable trade-offs to ensure these parameters are maximised.

### 2.2.5 Flanges

Unlike the design of the joints, the design of the flanges was straightforward and remained almost unchanged throughout the project. Initially, a parallel plate concept was investigated, where laser-cut aluminium plates were separated by spacers bolted to the plates (Fig. 2.13 - far left).

However, because the plates can have a maximum width of only 5mm because of laser cutting, the design was not stiff. Also, the plates were not wide enough to accommodate the end effector mechanism. Instead, an aluminium box-section was proposed. The advantages of using aluminium box sections are shown in Table 2.9:

Table 2.9: Advantages of Aluminium Box Section

Advantages of Aluminium Box Section
Readily available from multiple suppliers for cheap prices and well tolerated
Many different thicknesses and dimensions available
Highly interchangeable. Should the flange length need to be altered, a new piece of aluminium box section can easily be cut to the desired length and fastened to the connectors

Manufacturing is needed only to cut the desired length and mill clearance holes to attach to the connector

High second moment of area means less deflection

A 50.7 x 50.7 mm box section with 1.6 mm thickness was considered. To test its suitability, Eq. 2.7 was used to calculate the load required to cause a vertical deflection of 0.1 mm (the PDS requirement for repeatability of movement.)

$$\delta = \frac{WL_f^3}{3EI} \quad (2.7)$$

Where  $L_f$  is the length of the flange,  $W$  is the load in Newtons,  $E$  is the Young's modulus,  $I$  the second moment of area and  $\delta$  the deflection. By setting  $L_f$  as 0.3 m (the maximum range according to PDS) and modelling the length as a cantilever, it was determined that a mass of 9.87 kg would be required at the end of the cantilever to cause a vertical deflection of 0.1 mm. Given that the total weight of the structure was to be a maximum 4 kg, with a maximum payload of 200 g, it is therefore impossible given the PDS requirements to cause an end deflection of 0.1 mm. As not all of the weight will be concentrated at the end of the cantilever the end deflection is further reduced. Overall, this design was selected as it is a cost-effective option that provided high stiffness to the whole structure of the arm.

### 2.2.6 End Effector

An end effector was required to accommodate different types of applications and the extra two degrees of freedom (vertical movement in Z-axis and rotation about the Z axis) that was specified in the PDS. To keep within the budget and also maintain a high level of accuracy, a lead screw mechanism was selected for the vertical motion. For two degrees of freedom, two motors were required.

Initially, the mechanism was designed to have one degree of freedom (vertical movement in the Z-axis) and we could purchase a gripper with the rotational degree of freedom. However, this would heavily rely on designing around the attachment purchased and limit the degrees of freedom of the structure. Hence it was decided that the end effector required two degrees of freedom, regardless of the attachment.

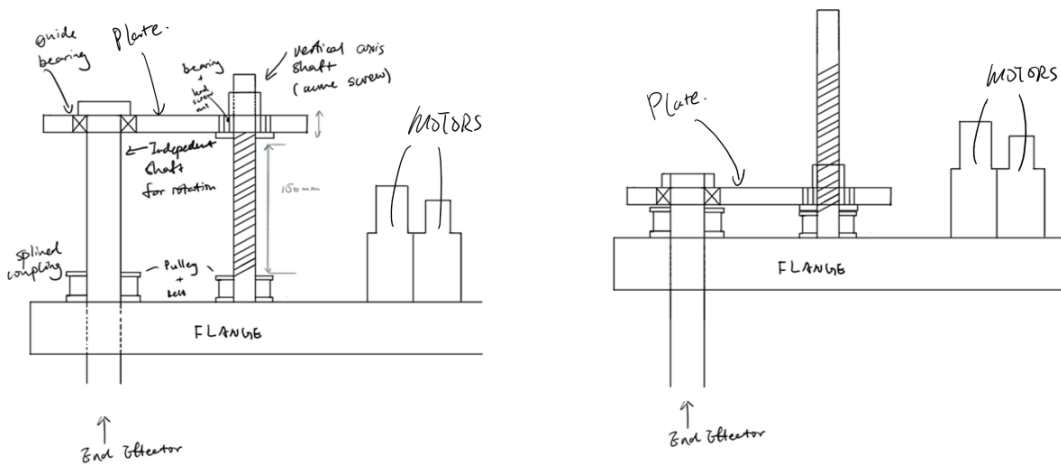


Figure 2.15: Initial Concept Sketch

An initial concept (seen in Fig. 2.15) was developed using a rod and an ACME screw that independently control each degree of freedom. The ACME screw is fixed relative to the plate as the screw nut is constrained in the plate. The rod was joined to the plate using a nut and bolt with a circular slot in the plate, hence allowing the rod to rotate but fixing it in the vertical direction.

When the ACME screw rotates, the nut is driven and hence the plate moves vertically up and down relative to the flange. Consequently, the rod connected to the plate also moves up and down. Therefore the vertical degree of freedom is achieved. As the rod is also attached to a pulley driven by a motor, with proper selection and control of the motor, a precise rotational step was achieved. After an initial review, three main issues were found as shown in Table 2.10 .

Table 2.10: Drawbacks to first iteration End Effector Design

Drawbacks to End Effector Design
With two motors placed on the same end of the flange, the flange length must be increased. Therefore the moment arm would increase causing overshoot when moving and reducing overall accuracy.
As the rod and ACME screw each control a degree of freedom, the rigidity of the structure would decrease as they are connected via a thin plate. The plate must resist torsional effects from the driving force and this can only be compensated with a much thicker plate which is unfeasible.
With two pairs of pulleys and belts requiring different tension values, two tensioners were needed. The flange has limited space and this may cause potential problems.

With the above in mind, the following improvements were made. It was determined that the force required for rotation of the rod is relatively small, hence the motor torque required for the rotational degree of freedom is smaller. Therefore this motor was directly joined to the rod with a

flex coupler. For maintaining the rigidity of the structure, a guide rod was required to resist torsional effects from the rotation of the ACME screw. In addition to the original top support plate, an extra bottom support plate was included, so that the guide rod moves with the plates. It was practical to drive the screw nut instead of the ACME screw hence the pulley that was attached to the screw is now attached to the nut.

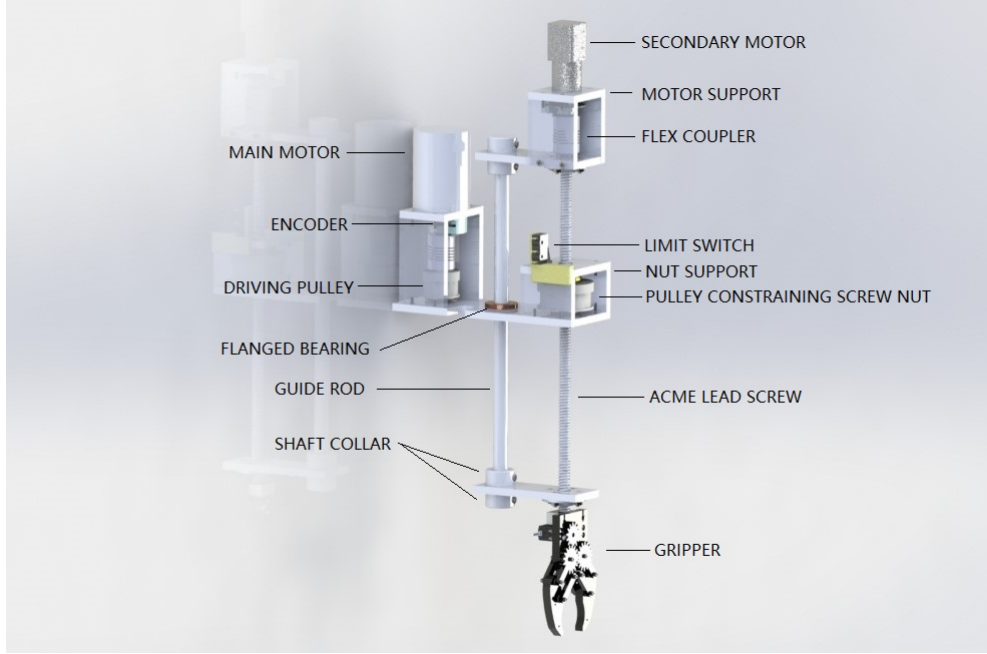


Figure 2.16: Updated Concept in CAD

An updated concept (shown in Fig. 2.16) was produced. The lead screw is driven by two motors alone, producing two degrees of freedom. The motor near the elbow joint drives the pulley, which is attached to the screw nut, through a timing belt. The screw nut was constrained in the axial direction of the lead screw so that it can drives the lead screw linearly. The motor coupled to the lead screw by a flex coupler is controlling the rotation of the lead screw. Minor vertical displacements of the lead screw arrangement occur during rotation, however, this can be compensated with the other motor to offset the difference. With the guide rod supporting the motion of the lead screw, overall rigidity was improved.

Standard Gripper Kit A was chosen as it demonstrates only open and close function. With its simplicity to detach, it can be easily replaced with other applications. [20]

The position of the adjustable tensioner can be set during assembly. A slot was created on the plate and flange, allowing the insertion of a shoulder bolt inside a bush bearing (similar to the transmission). Factoring manufacturing considerations into the design process, further changes were implemented to several components. The nut support and motor supports (as shown in Fig.

2.17 were divided into three separate plates and joined using countersunk flat head screws.



Figure 2.17: Example Motor Support

### 2.2.7 Cover and Wiring

Fig. 2.18 shows the robot with the cover on.

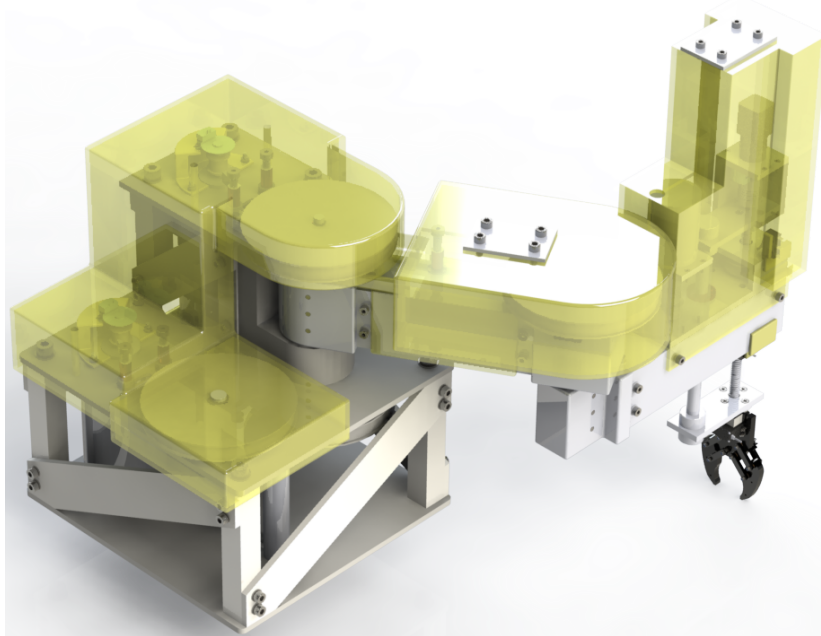


Figure 2.18: Robot with Cover

The cover was essential for the longevity and safety of the robot. The component most susceptible to damage in the robot is the encoder. If the encoder is not shielded from dust, the accuracy of the robot will degrade as dust collects. Therefore, the cover was designed to limit exposure to the

encoder. Additionally, as the motors are operating at 80W, exposed transmission components constitute a safety hazard. As such, the cover was designed to form a shield over the exposed transmission components. The cover was in 3 parts: Base, Flange and End-effector covers.

The base cover was assembled on the robot from above. The ends clamp onto the base, fixing it in the XY plane. Three pillars protrude from the top near the encoder mounts, which hold it in the Z direction. Barring the bottom of the pulley (which is on the 2<sup>nd</sup> level of the base), the cover envelopes all transmission components. The gap between the pulley and the cover is minimal, therefore if dust enters the probability of damage to the encoders is low.

The flange cover was attached from the sides and bolted at the top. The sides clamp onto the plate, fixing it vertically. The fixing at the top prevents XY motion. The screws bolting the flange and the joints together provide additional support as they squeeze the cover between them. There are open slots (like the ones for the idlers) at the top which allow the bolt-plate to be slid onto the flange cover; the idea is that one of the flange covers is put on first. Then the bolt plate is bolted onto it. Then the second flange cover is attached and slid onto the bolt plate. The screws are then reverse tightened.

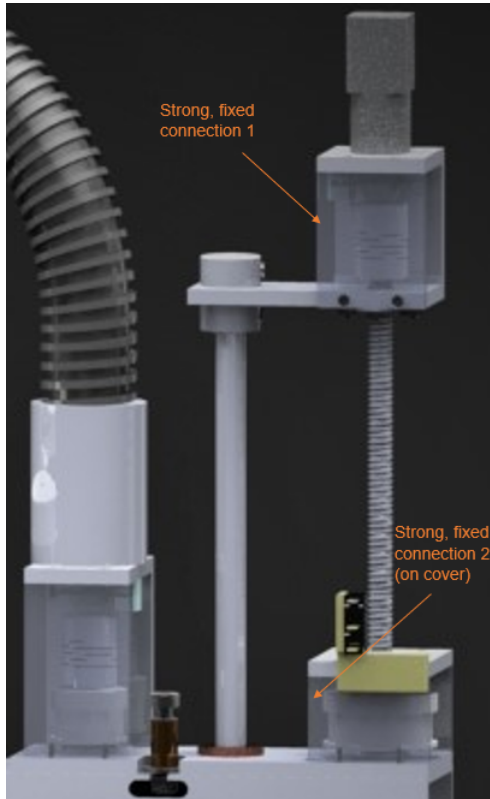


Figure 2.19: End-Effector with conduit

The end effector cover was similar to the flange cover in terms of assembly. The only difference was that it is bolted onto the flange. In terms of protection, the only openings to the internal components are through the holes at the bottom for the lead screw and guide rod. A potential way dust could enter is by attaching onto the lead screw or guide rod as they are lifted. The system is therefore minimally exposed to the environment but regular cleaning will mitigate any adverse impacts. The electronics (except the power supplies and encoders) are located under the base of the robot. The wiring has 2 parts - wires from the base and flange and wires from the end-effector.

There is a small opening for wires at the bottom of the covers. Wires from the limit switch are taped along the flange and fed out through the opening into the base. The wires from the base and flange were fed through holes in the structure. The wiring

from the flange was taped to the base and then fed into the electronics. Slack is afforded in wiring to allow for motion of the shoulder.

The wiring from the end-effector was fed into the electronics via a conduit (in Fig. 2.19) which is mounted at the top of the end-effector cover, on the horizontal surface immediately below the bolt-plate (and at the base at the other end). Wires coming from moving components of the end-effector (i.e. the motor controlling angular motion and its corresponding encoder) are taped tightly to the motor support and a hook on the inside of the cover(near the limit switch), creating strong, fixed connections at those points. Slack was once again incorporated between those points (points 1 and 2 in Fig. 2.19) for the vertical motion of the end-effector. From that connection point at the cover, the wires are guided to the conduit along hooks in the cover.

### 2.3 Electrical Design

Fig. 2.20 shows the basic components in the control loop.

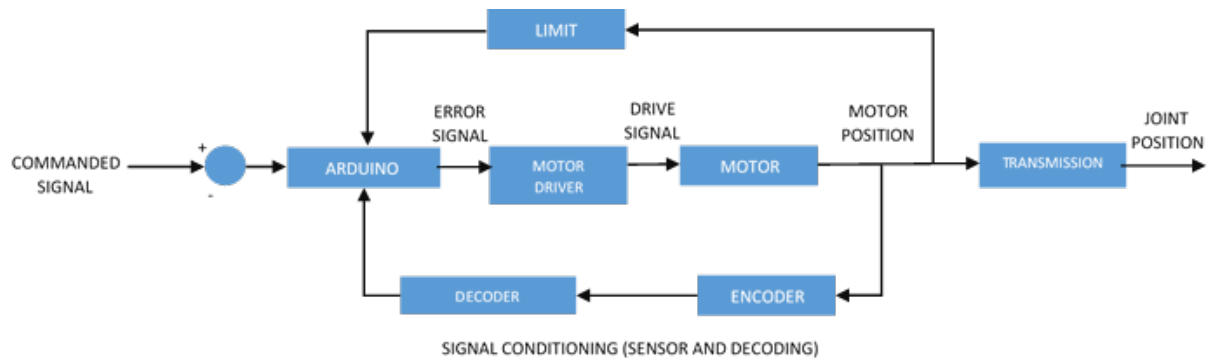


Figure 2.20: Block Diagram of Control System

#### 2.3.1 Encoder

Position feedback was received by attaching an encoder and sending its signals, via a decoder, to the Arduino. Considering the stress on accuracy of the robot, an encoder with a high resolution was preferable. However, as the price of encoders increases with encoder resolution, due to budget constraints, balance is required. The AEDB-9140-A13 Encoder was chosen.

Table 2.11: Operating Parameters of Encoder [21]

Parameter	Value
Temperature	-10 to 85 °C
Supply Voltage	4.5 to 5.5 V
Max Frequency	100 kHz
Supply Current	30 to 85 mA
Rise Time	180 ns
Fall Time	50 ns



Figure 2.21: Encoder Outputs [21]

The two-channel encoder has a resolution of 500 pulses per revolution, allowing for maximum accuracy of 0.18°. The encoder costs approximately £30, which would total to £120 for the whole robot, at the time of selection most encoders with poorer resolution had a similar price range. Prices of encoders with higher resolution were all over £50, which exceeded our budget.

The encoder has 3 outputs; Channel A, Channel B and Channel I. A and B are ninety degrees out of phase, with A leading B if the motor is spinning clockwise and B leading A if anti-clockwise. Channel I pulses every time the encoder makes a complete revolution. This is shown in Fig. 2.22. Table 2.11 shows its operating parameters.

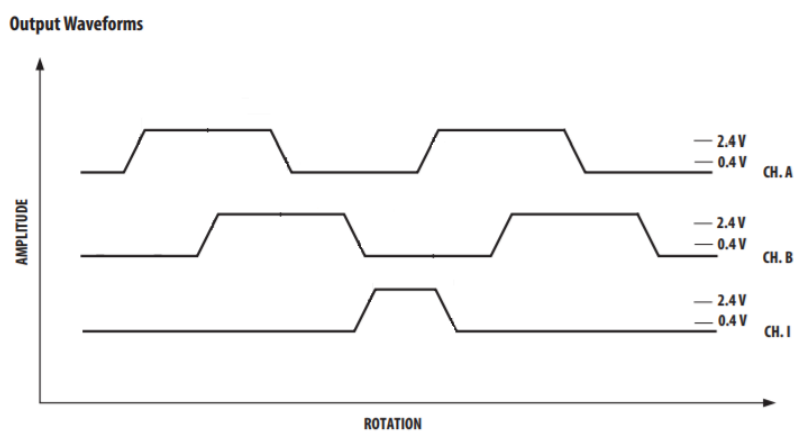


Figure 2.22: Encoder Outputs [21]

### 2.3.2 Decoder

For the decoder, the HCTL-2016 was chosen. Fig. 2.24 shows the pin-out of the integrated circuit. Table 2.12 shows the decoders operating parameters.

Table 2.12: Operating Parameters [HCTL-2016] [22]

Parameter	Value
Operating Voltage	5 V
Max Frequency	14 MHz
Temperature	-40 to 85 °C
Counter Size	16 bits

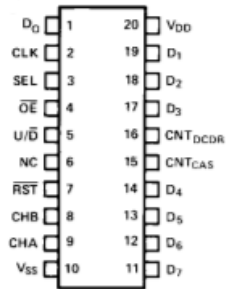


Figure 2.23: HCTL-2016 Pinout [23]

The HCTL-2016 is a combined quadrature decoder and 16 bit counter which can support clock frequencies of up to 14 MHz. Table 2.13 explains the functions of each of the pins.

Table 2.13: Pin Functions [23]

Symbol	Function
$V_{DD}$	Power Supply
$V_{SS}$	Ground
$CLK$	Input for external clock
$CHA/B$	Input for encoder Channel A/B
$\overline{RST}$	Reset pin (clears internal position)
$\overline{OE}$	Output Enable pin, must be kept at an active low
$SEL$	Controls which bits are displayed at output. Keep at 1 for first 8 bits
$CNT_{DCDR}$	Output which pulses on change of state
$U/\overline{D}$	Output which indicates whether counter is counting up or down
$CNT_{CAS}$	Output which pulses on counter overflow
$NC$	Not Connected/Don't care
$D_{0-7}$	Output bits

For this application, the clock input is provided by a 12 MHz Crystal (Fig. 2.24), connected as per Fig. 2.24 (the 3.3 V comes from the Arduino Mega). The Arduino reads the value of the change in position through pins  $D_{0-7}$ . A separate oscillator/timer circuit will be connected to the  $\overline{SEL}$  pin to swap between the upper and lower bytes, at the Arduino's sampling frequency. The value of this oscillator was estimated to be approximately 0.3 MHz (see Section 5.2.2) but will require testing to verify.

Note that the HCTL-2016 is but one of many possible decoders that could be used. It performs the required functions that the control loop demands of it and is cheap (approximately £1.5), going through the trouble of finding a cheaper or better performing decoder was deemed unnecessary.

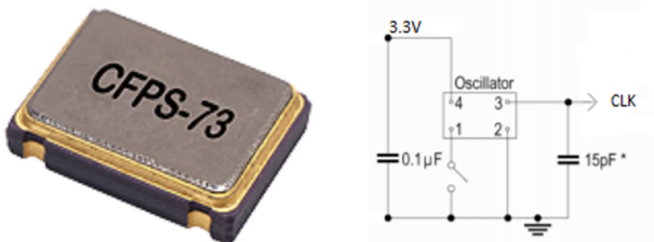


Figure 2.24: **Left**: CFPS-73 Crystal [24], **Right**: Oscillator Circuit [24]

The decoder has three inputs (CHA, CHB, CLK) and eight outputs (D0-D7). Additionally, only one encoder is sampled per decoder. To reduce the wiring and number of components, communication via a separate micro-controller (which would decode the encoder pulses and send them to the Arduino) was considered.

Serial communication (such as UART, I2C and SPI protocols) transfers data bit by bit over the same data bus, thus reducing the number of pins and wires utilised. In contrast, parallel communication transfers all bits simultaneously, over a greater number of pins. Both methods have advantages and disadvantages which are weighted relative to each other in Table 2.14.

Table 2.14: Comparison of Serial and Parallel Communication [25]

Factor	Serial Communication	Parallel Communication
Transmission Speed (For 'N' bits)	N clock cycles	1 clock cycle
Cost	Lower cost due to less hardware	Higher costs due to greater hardware
Frequency Bandwidth	High	Low
Programmability	Difficult	Easier
Transfer Distance	Less susceptible to noise and corruption at distance	More susceptible to noise and corruption at distance

Comparing the two types of communication, it was concluded that parallel communication using counters would be the more appropriate protocol. This conclusion was largely drawn due to the nature of the application. The requirement for a quick response of the control system was the major deciding factor, as waiting for multiple clock cycles to read position data may lead to misrepresentation of the feedback. Additionally, the sampling rate of micro-controllers cannot match the frequency of the encoder pulses, resulting in the loss of pulses. This is explored further in Sections 4.1.2 and 5.2.2.

Although using parallel communication with counters may incur greater costs, at the physical scale of the robot control system, the difference in costs was considered negligible. Finally, given the short physical range of data transfer, chances of noise and corruption affecting the signal are reduced. Thus for the feedback signals, parallel communication was utilised.

### 2.3.3 Motor Driver

In order to control a motor rated at 24 V and 3 A, the Adafruit DRV8871 was chosen as it could handle up to 50 V and 3.5 A [26]. Table 2.15 shows its Operating Parameters.

Table 2.15: Operating Parameters of DRV8871[26]

Parameter	Value
Power Supply Voltage	-0.3 to 50 V
Logic input voltage	-0.3 to 7 V
Output Current (at 100% duty cycle)	0 to 3.5 A
Temperature	-40 to 150 °C

A depiction of the breakout board and the motor driver schematics are shown in Fig. 2.25.

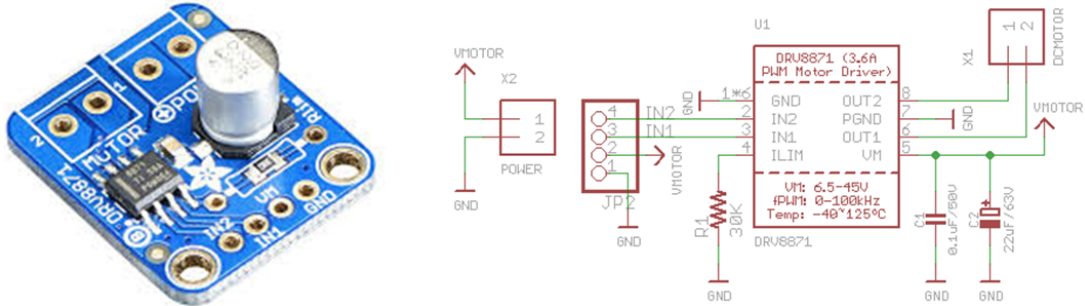


Figure 2.25: **Left:** DRV8871 Board[26], **Right:** DRV8871 Schematic[26]

The motor is controlled via input signals from IN1 and IN2, which act as switches, allowing current to flow in a certain way. Table 2.16 shows the DRV8871's truth table.

Table 2.16: DRV8871 Motor Driver Truth Table [26]

IN1	IN2	OUT1	OUT2	Description
0	0	H	H	Coasting
0	1	L	H	Reverse
1	0	H	L	Forward
1	1	L	L	Brake

Fig. 2.26 shows the corresponding current paths for all the states of the truth table.

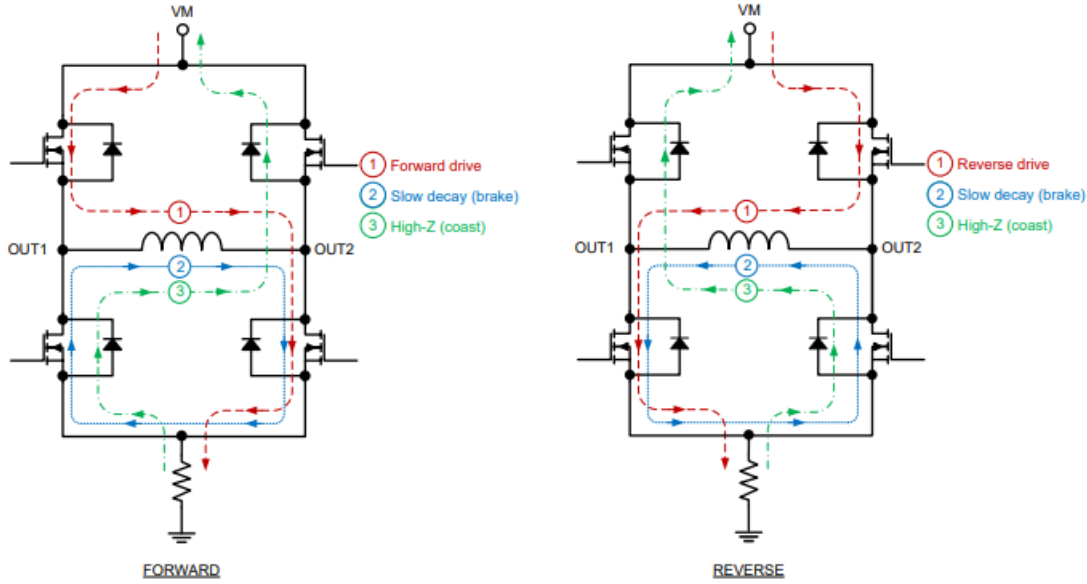


Figure 2.26: DRV8871 Current Paths [26]

Using the truth-table, motor control can be achieved by manipulating IN1 and IN2.

#### 2.3.4 Limit Switch

Should a program which requires the arm to move out of its range of motion (and crash into the body of the robot) be accidentally written, a limit switch (Fig. 2.27) was utilised to force the motor to stop. This was an electrical stop which triggers a break in the circuit - stopping the program from executing temporarily. By putting these on the ends of the range of motion, they will stop all programs when the arm (or end effector) reaches the end of its motion, preventing crashes and motor overheating (as a result of trying to push the arm into the body of the robot). The limit switch has 3 pins - one on the far left of Fig. 2.27 (COM), one in the middle (NO), and one on the far right (NC). COM is connected to a voltage source and NO is connected to the Arduino. NO returns a low (0) to the micro-controller while the limit switch is unpressed and a high (1) if pressed. NC does the opposite of NO and was left unconnected in the application.



Figure 2.27: Limit Switch

#### 2.3.5 Arduino Mega 2560 R3

The Arduino Mega 2560 R3 was chosen as the controller for this project. Table 2.17 gives the technical specifications of the Mega.

Table 2.17: Arduino Mega 2560 Technical Specifications

Parameter	Value
Operating Voltage	5 V
Digital I/O Pins	54 (of which 15 provide a PWM output)
Analog I/O Pins (can also be used as Digital)	16
DC Current per I/O Pin	20 mA
Flash Memory	256 kB (8 kB used by bootloader)
Clock Speed	16 MHz

Fig. 2.28 shows the Arduino connections with all the other components of the control loop to drive one motor (neglecting power supply rails). Eight (I/O) pins will be needed for the decoder output, one pin for resetting the decoder ( $\overline{RST}$  pin), one pin for Channel I of the encoder, one pin for the limit switch and two PWM pins for the motor driver. This makes a total of thirteen pins, resulting in fifty-two pins required for running four motors.

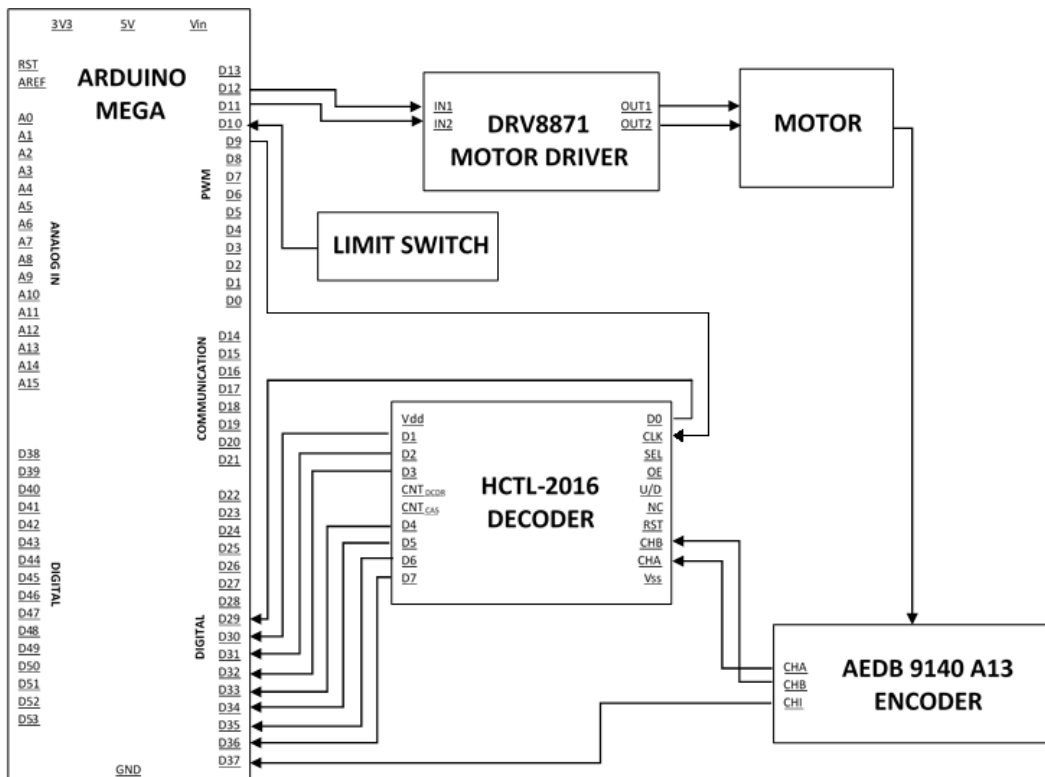


Figure 2.28: Arduino Mega in connection with Control System

As per the specifications, a total of seventy pins are available for use. Eighteen pins are unused (of which seven provide PWM output). This way, even if the number of pins required increases later on, the Arduino can accommodate them.

### 2.3.6 Power Supply System

To drive the system, an energy source in the form of a power supply is crucial. Each component within the electronic infrastructure of the robot requires energy to operate and understanding the power requirements of each component assists in the selection of an appropriate power source.

Power adds up in a circuit regardless of configuration, therefore the power demands of the system are tabulated in Table 2.18:

Table 2.18: Rated Characteristics of System Components [14][15][26][27]

Component	Rated Power	Rated Voltage	Rated Current	Quantity	Total Power
Joint Motor	80 W	24 V	3 A	2	160 W
End Effector Motor	7.2 W	12 V	0.6 A	2	14.4 W
Limit Switch	3.6 W	12 V	0.3 A	2	7.2 W
Motor Driver	0.072 W	24 V	3 mA	4	0.288 W
Encoder	0.285 W	5 V	57 mA	4	1.14 W
Decoder	5 $\mu$ W	5 V	1 $\mu$ A	4	20 $\mu$ W
Arduino Mega	5 W	5 V	1 A	1	5 W
Total					188 W

The values in italics were extrapolated using the stated datasheet parameters and the appropriate formulation of Joule's First Law ( $P = IV$ ). Two key considerations for power supply selection were determined from Table 2.18. First, a minimum of 188 W was required to drive the system.

Additionally, there were three distinct voltage rails required: + 5 V, + 12 V and + 24 V. Thus identifying a power supply with the three voltage rails readily accessible would be beneficial, to prevent the need for the design of voltage regulator circuitry. A major limitation of multi-voltage power supplies is the power available for each rail, thus a deeper analysis of the power demanded by each voltage rail was required (see Table 2.19):

Table 2.19: Total Power by Voltage Rail

Voltage Rail	5 V	12 V	24 V
Total Power	6.4 W	21.6 W	160.288 W

The large 160 W demand from the 24 V rail was not readily met with a single multi-voltage power supply when taking into consideration the available budget and the overall system power efficiency. Therefore the unconventional decision was made to have two separate power supplies. Two Mean Well RS-125D power supplies provided the necessary characteristics to power the system. The

characteristics of the power supply are shown in Table 2.20:

Table 2.20: RS-125D Power Supply Specifications [28]

Model		RS-125D	
Output Number	CH1	CH2	CH3
DC Voltage	+5 V	+24 V	+12 V
Rated Current	8 A	3 A	2 A
Current Range	2 - 15 A	0.4 - 4 A	0.1 - 2 A
Rated Power	136 W		

With two RS-125D's, the power requirements are fulfilled. The power distribution between channels must not exceed 136 W in total (272 W overall). The power available in the 24 V rail is applied to the motor and motor drivers. The motor and drivers are in a parallel configuration. Although the motor is not running at its nominal ratings due to the limits of the power supply, the current draw across the motor drivers is negligible so overall performance was expected to be unaffected. For the 12 V rail and 5 V rails, appropriate current regulators were developed to drive the encoder, end effector motors, limit switches, decoder and Arduino Mega at the appropriate currents.

### 2.3.7 Graphical User Interface

A slider graphical user interface (GUI) was developed as a method to provide the user demanded joint position. Each degree of freedom can be independently controlled by a slider as shown in the wireframe (Fig 2.29) below.

The values set by the sliders need to be accessed by the Arduino by a communication protocol. There were several GUI design softwares capable of providing this functionality. Four of such software were investigated: Microsoft Visual Studio, LabView, Processing IDE and MATLAB. Each had advantages and disadvantages, however, the sheer number of resources available to support development consolidated the selection of Processing IDE.

Processing has an intuitive development platform, similar to that of the Arduino IDE. The GUI communicates with the microprocessor via serial communication, utilising the serial library available in processing. Additionally, the dynamic visual elements, such as sliders and buttons, were implemented using the ControlP5 library.

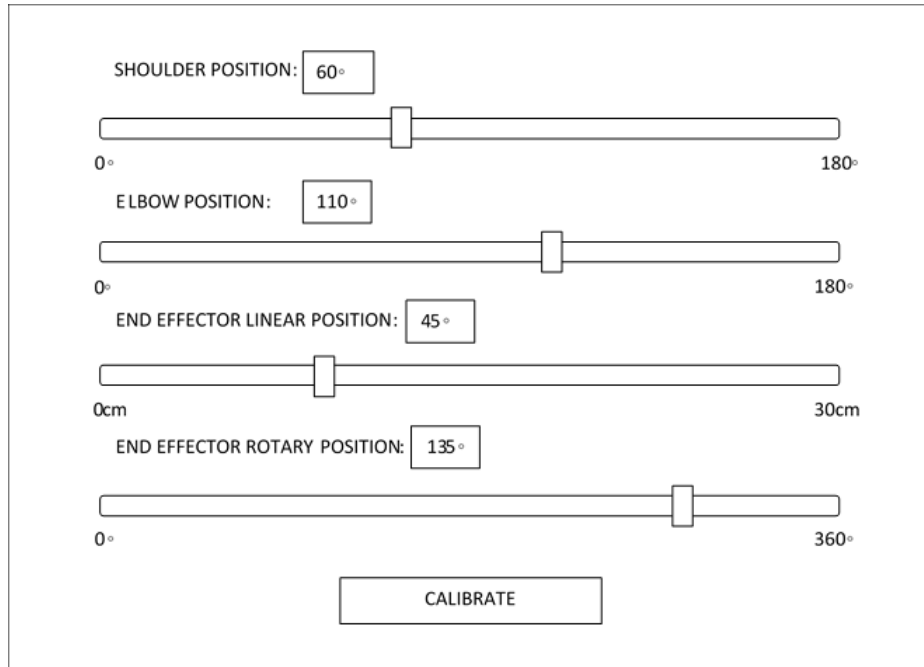


Figure 2.29: Wireframe of Slider GUI

### 2.3.8 Integrated System

The individual components were integrated to form the robot's control system. Table 2.21 highlights the methodology and data flow in the control system for one degree of freedom:

Table 2.21: Data Flow in Control System

Component	Data Input(s)	Process	Data Output(s)
AEDB-9140-A13 Encoder	Voltage signals (from photosensors and LED pairing)	Generates boolean pulses based on photosensor readings due to light exposure at code wheel intervals that contains direction and positional information	CHA, CHB & CHI
HCTL-2016 Decoder	CHA, CHB (from encoder) Clock Signal CK (from crystal) $\overline{RST}$ (from Arduino)	Decodes encoder signals to discern direction of motor. An embedded counter tracks position via pulses depending on the UP/DOWN signal generated by the decoding logic	D0-D7 (Output Count/Position)

Arduino Mega 2560 R3	CHI (from encoder)  D0-D7 (from decoder)  Limit Switch  Voltage	Converts binary data from decoder into decimal count. Uses conversion formula to determine motor shaft position. Compares feedback to demanded position to compute error signal. Outputs signal to motor drivers dependent on value of error signal. Cuts motion if limit switch is triggered	IN1 & IN2  $\overline{RST}$ (to decoder)
DRV8871 Motor Driver	IN1 & IN2 (from Arduino)	Utilises input signals to drive H-Bridge circuit for motor control	OUT1 & OUT2
Motor	OUT1 & OUT2 (from motor driver)	Drives motor clockwise or anticlockwise depending on input signals from drivers	-

While most of the components are hardware-driven, the control algorithm developed on the Arduino was software-based. An expansion of the basic algorithm for one degree of freedom is depicted in the flowchart shown in Fig. 2.30.

The same methodology can be applied to all other degrees of freedom. After configuring the appropriate ports/registers and initialising the required variables, the system accepts the output of the decoder, the commanded position from the GUI and the state of the limit switch. The limit switch is on an interrupt, triggering an interrupt service routine (ISR) when the input is high, thus providing more efficient use of the CPU. The ISR is depicted in Fig. 2.30.

Assuming the interrupt flag has not been raised, the algorithm first assembles the received bits from the counter into one byte, representing the total number of counts received. This value is then converted to degrees by multiplying through by the graduation angle, as described by Eq. 2.8:

$$\theta = \theta_p \left( \sum_i^{CCW} N_i - \sum_j^{CW} N_j \right) = \theta_p N \quad (2.8)$$

Given the position fed-back by the encoders, the error signal can then be computed by subtracting the feedback position from the commanded position. The value of the error signal is utilised to drive the motor in the direction to fix the error (if the error is greater than zero, the system has undershot hence set IN1 and IN2 to drive clockwise and vice versa). This process is repeated until the error signal reads zero (or is within a small threshold band around zero depending on test results).

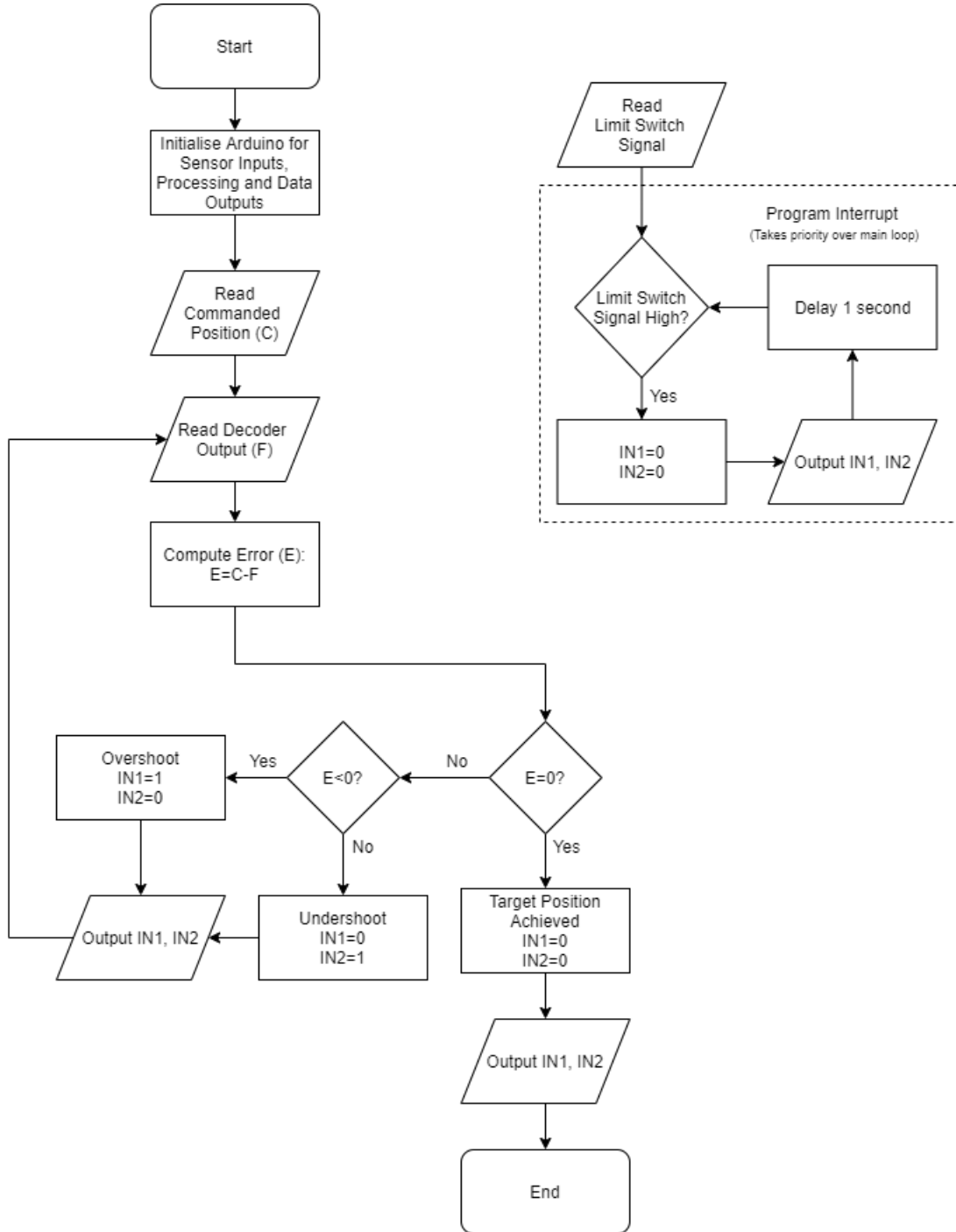


Figure 2.30: Control Algorithm Flowchart

The initialisation routine (the first block after start in Fig. 2.30) is depicted in Fig. 2.31.

On start-up, the motor is moved (at low speed) till it hits a limit switch. Then it is moved in the opposite direction until a pulse is received from channel I (of the encoder). Then the motor is stopped and a pulse is sent from the Arduino to the RST pin of the decoder, calibrating that as its starting position. All following calculations are carried out from reference to that point (for example, commanded position of 30° is 30° from that point).

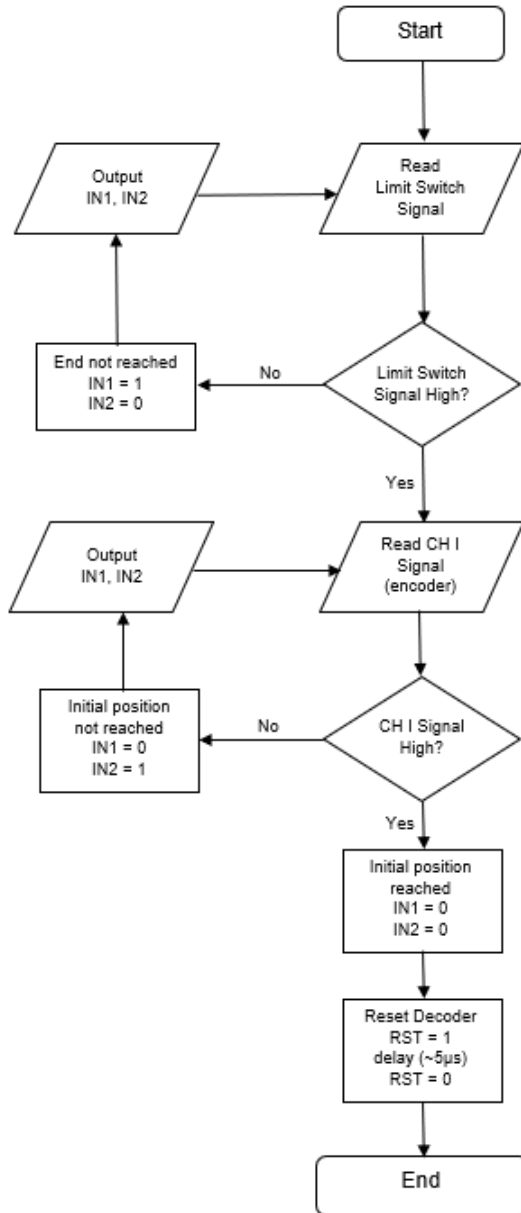


Figure 2.31: Initialisation Routine Flowchart

The algorithm and system response was to be analysed via testing in the summer term, however, due to Coronavirus, this could not be completed (see Section 5).

### 3 Manufacturing Phase

This section provides a summary of the manufacturing of the robot. Tools and methodologies used for critical components are introduced. With consideration of future design iterations, manufacturing was divided into modular sub-assemblies. The sub-assemblies are detailed in the following subsections.

### 3.1 Base

The mounting plates and side plates are made of 5 mm thick aluminium alloy (5251H22) sheets. Since they contain holes which position the shafts and motors with moderate tolerances ( $\pm 0.5$  mm), laser cutting was requested for these components.

Four supporting pillars were machined on a mill in the mechanical engineering student teaching workshop (STW) using an aluminium square bar (6082T6) with a side length of 20 mm. Then as designed, M8 and M5 socket head cap screws were used for the base structure of sub-assembly, as shown in Fig. 3.1.

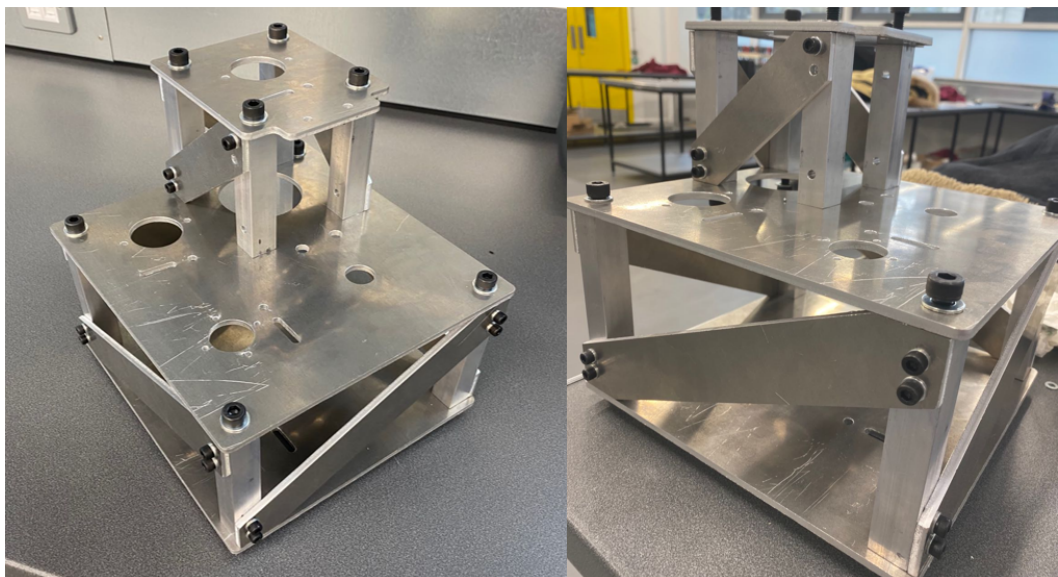


Figure 3.1: Picture of Assembled Base Structure

### 3.2 Transmission

All transmission elements in the robot follow the same concept: a two-stage reduction involving pulleys and timing belts. Each stage has a 6:1 reduction ratio and four main parts: the pulley, the shaft, the idlers and timing belt.

**Timing belt:** These were purchased straight from a supplier and needed no further work.

**Idler:** Each idler was made of 3 simple components that needed no further work. The three components and the corresponding tolerances are M6 x 12.5 shoulder bolts (f9 tolerance), 6 mm diameter oilite bush bearing (G7 tolerance) and an M5 Nut. G7/f9 is a loose clearance fit hence the oilite bush bearing can freely rotate on the shoulder bolt. The shoulder bolt was attached to the base/flange by tightening the M5 nut (See Fig. 2.8).

**Pulleys:** The purchased pulleys are delivered with bosses, which are required to be removed with a mill. The bore size of the pulleys was required to be 8 mm, except for one 72 tooth pulley that was bored to a 12 mm diameter. All tolerances were H7 to ensure a tight H7/g6 fit on the shafts. The pulleys were constrained axially with circlips and shoulders on the shaft. Keys were employed as the method for rotational constraint.

**Shafts:** All shafts were manufactured on a lathe with 16mm diameter mild steel EN1A available from ME Stores.

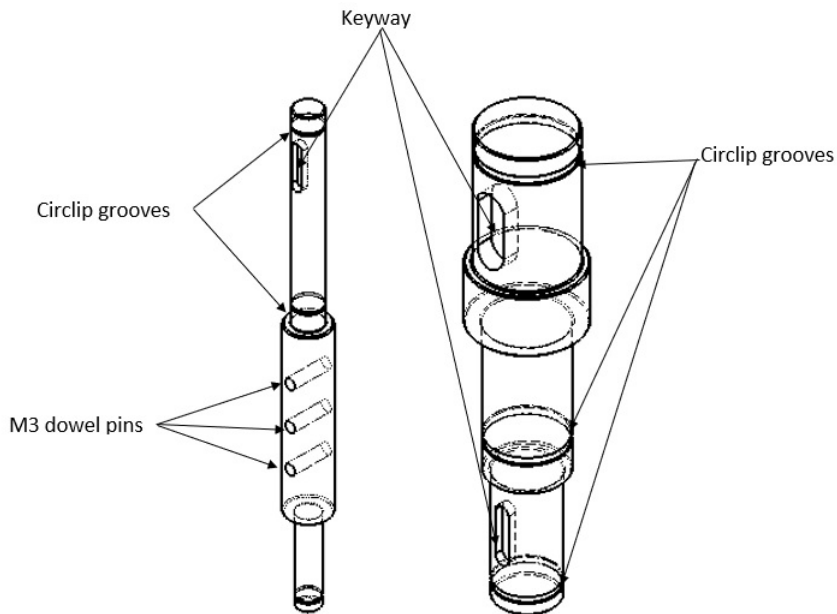


Figure 3.2: Shaft examples **Left:** Shoulder shaft **Right:** Intermediate shaft

The keyways were cut using a mill with dimensions/tolerances according to BS-4235 [29]. The circlip grooves were cut according to BS-3693 on a lathe with a circlip groove cutting tool. For the dowel pin holes, the shafts were placed inside the connectors and cut together on a mill to ensure perfect alignment. A g6 tolerance was used on the parts that would accommodate a pulley or a connector and all other parts were toleranced to  $\pm 0.5$  mm.

Lastly, the keys were cut with a handsaw and filed down in the IDEAs workspace. A trial and error method was used until the keys were filed down enough to fit with an interference fit into the keyways.

### 3.3 Joints

**Shoulder joint:** The manufacturing of the shoulder joint support was problematic due to its size. If it is machined from one piece of metal, it would require a solid square bar with side lengths of

100 mm, which is not available in Imperial College Mechanical Engineering Store (Mech Store) and expensive from external suppliers, and a huge proportion of the metal is machined off. Therefore, an alternative procedure was taken, as shown on the right side of Fig. 3.3.

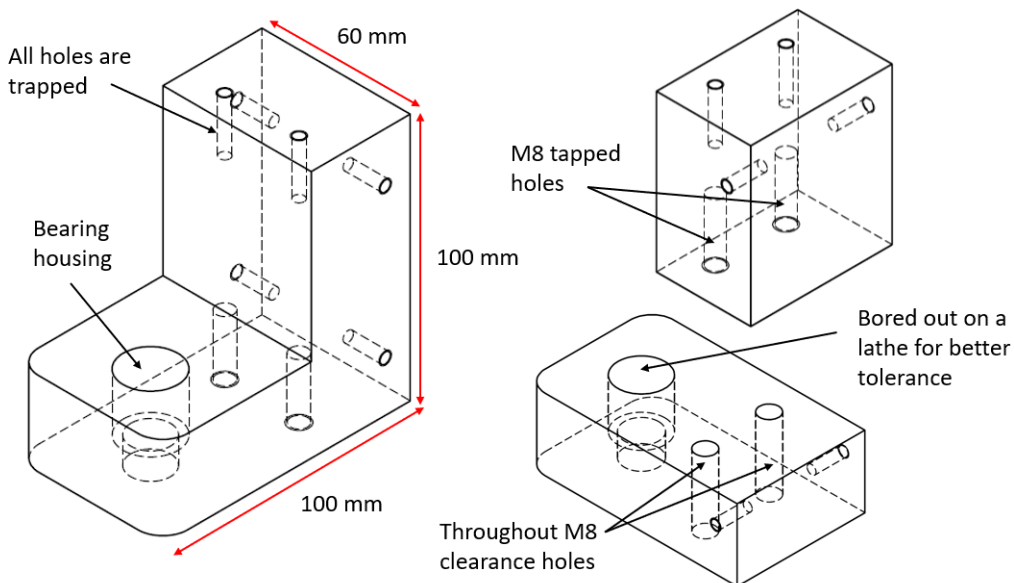


Figure 3.3: **Left:** Original design of the component, **Right:** Manufactured parts

The originally designed component were divided into two rectangular parts to be machined from 60 mm aluminium square bar (6082T6) supplied by Mech Stores. Both blocks were machined to size on a mill. The positions for holes were determined at the same stage. The bearing housing is bored out on a lathe for the designed H7 tolerance. For assembly, the two blocks were to be clamped together by the top and lower mounting plates and fixed by M8 socket head cap screws. The manufacturing costs and difficulty are therefore significantly lowered, without compromising the performance of the critical component.

Note that the shoulder connector was made in the same way as the upper connector (explained below) but without the bearings housings and M3 x 15 tapped holes.

**Elbow joint:** Each connector in the elbow joint was manufactured from solid 60 x 60 mm aluminium (6082T6) square bar available from ME stores. The material was cut to 80 mm length, and machine work was conducted on a mill and lathe. To save time, we considered using CNC methods to manufacture the connectors, but this method was rejected due to the long waiting times to use Imperial's CNC facilities (6 weeks minimum waiting time) and the high cost of using external CNC services (around £350 per piece).

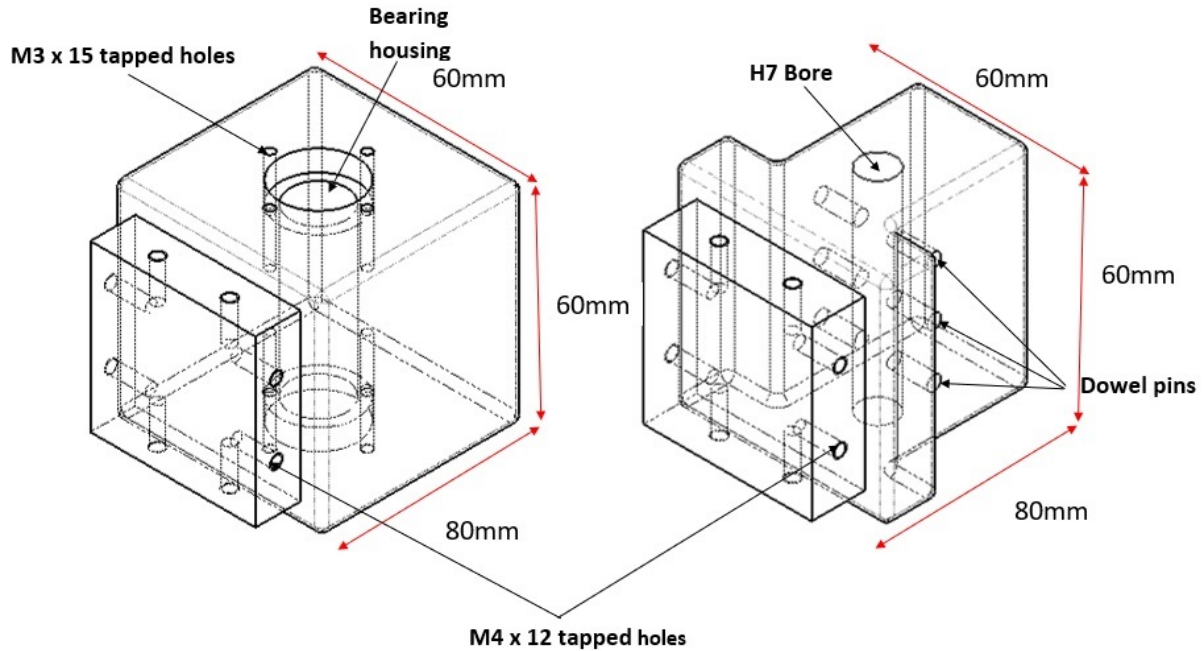


Figure 3.4: Elbow connectors **Left:** Upper connector **Right:** Lower connector

The most complex aspect of manufacturing was the bearing housing in the upper connector (Fig. 3.4). The part was made by placing the connector on a four-jaw chuck in a lathe. As a critical part of the entire design, the tolerance is extremely tight as the bearing must be fixed both axially and rotationally. In practice, this is equivalent to a tight fit (transition fit), such as a H7/j6. However, instead of blindly aiming for a H7/j6 tolerance and hoping that the bearing is tightly housed, an arduous trial and error method was utilised. Five micrometres of diameters were turned on the lathe until the bearing fit tightly into the housing. Apart from the bearing housings, all other features of the connectors were manufactured on the mill, including both the removal of material and tapping of holes.

To ensure a tight fit (H7/j6) between the connector and the flanges a similar trial and error method was used. Ten micrometres of the material was turned at a time until the aluminium box-section had a tight fit with the connector. Overall, two out of the three connections had a tight fit, but the last connection had notable play. The impact was minimised due to the tight fastening of the M4 bolts, which keep the connection between the flange and the connector stiff and rigid.

To ensure a H7 tolerance for the bore on the lower connector, a H7 reamer was used from STW. Once this was completed the three dowel holes were drilled along with the connectors using a 3 mm drill bit.

### 3.4 Flanges

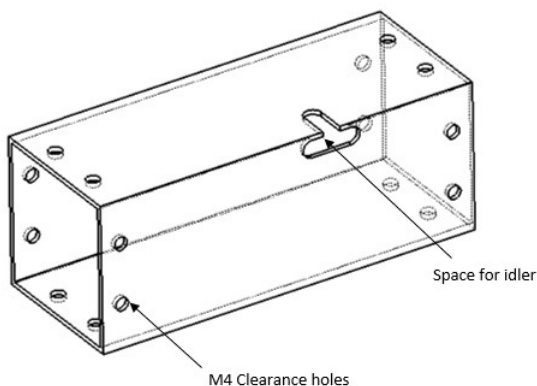


Figure 3.5: Flange connecting shoulder to upper connector

Compared to the connectors, the manufacture and assembly of the flanges was a fairly straightforward process. As previously mentioned, the flanges are aluminium box sections cut to the required length in the STW. From this stage, completion of the flanges is contingent on two more steps.

1. **Drill clearance holes:** For the flanges to attach to the connectors, clearance holes were drilled for the M4 bolts. By utilising the coordinate features of the mill, the holes were mapped and drilled. This method produced misalignment between the clearance holes on the flanges and the tapped holes in the connectors. The greatest error was roughly 1 mm off centre. For one hole, the M4 x 12 bolt could not pass through the clearance hole. The clearance hole was expanded by manually filing to rectify the problem. A better method would have been to place the aluminium box-section onto the connector and drill through both simultaneously, thereby ensuring perfect alignment. This method was used when drilling the holes for the dowel pins through the connectors and the shaft with great success.
2. **Drill space for idlers:** An idler was required for the timing belt on the flange, between the shoulder and upper connector. Hence space for it was milled (See Fig. 3.5). The space was designed so that the position of the idler can be adjusted to tighten the timing belt while allowing adequate space for a wrench to tighten the nut to keep the idler firmly in place.

Once the above was done, the flanges were fitted on to the connectors and fixed in place with M4 x 12 bolts and washers.

### 3.5 End Effector

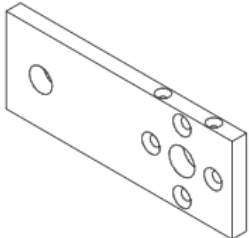


Figure 3.6: Example plate

The end effector consists of ninety six components including purchased components, nuts and screws. However, only nineteen components need to be manufactured including twelve plates, two bearing housings, three shafts and modification to two pulleys. The plates should have been manufactured first. The M2 and M3 holes that join the plates together have a tolerance of  $\pm 0.1$  mm. The M5 clearance holes that join the centre plate to the flange have a tolerance of  $\pm 0.15$  mm. As there are multiple holes on the plates with

their centre location being most crucial, laser cutting technique was implemented. Plates with correct dimensions and hole locations are obtained.

Most of the holes required internal threading and some required the countersunk feature. This work was carried out using the mill. The laser cutting etched the locations of the holes on the plate. M2 and M3 holes were drilled to  $1.6 \pm 0.1$  mm and  $2.5 \pm 0.1$  mm respectively then threading taps were used to create internal threading. The design required a specialist M2 tapping set that was not available in the STW, thus needed to be ordered separately.

While waiting for the threading set to arrive, two bearing housings were made on the lathe from an aluminium rod. The rod was fixed in the headstock and faced down using a 30-degree sharp-edged tool. The dimensions produced electronically on the lathe were repeatedly checked against manual measurement using a bore gauge. After the sections were faced to correct dimensions, the partition tool was used to separate the machined part from the raw material. The machined piece was taken down and fixed in with the cut off face facing outwards. A smaller drill was placed in the tailstock. A through-hole allowed the shaft to pass through, then a larger drill was used for creating the area to contain the bearing.

By the time the M2 tapping set was delivered, the workshop was closed and no further work could be carried out. Further manufacturing includes threading of holes, turning the shaft down on a mill and boring out pulleys to correct dimensions to fit the nut and shaft.

After manufacturing all the components, the end effector is to be assembled in the following order:

1. Assemble motor supports with M2 screws. Attach motors and encoder assemblies onto motor supports. Fix flex couplers onto motor shafts.
2. Assemble nut support with M2 screws. Constrain nut in the corresponding pulley with lead

screw and spacers.

3. Align with nut support and fix nut support onto centre plate. Attach limit switch.
4. Assemble top plate with lead screw through. Fix motor support to top plate.
5. Assemble bottom plate with lead screw through and attach gripper.
6. Insert the guide rod through the flanged bearing and fix to top and bottom plate using shaft collars and grub screws at pre-drilled locations.
7. Fix bearing and pulley with the extra shaft onto the centre plate.
8. Fix assembled motor support onto centre plate using M3 screws.
9. Attach belt tensioner and adjust timing belt tension to required value after fixing the assembly to the flange.

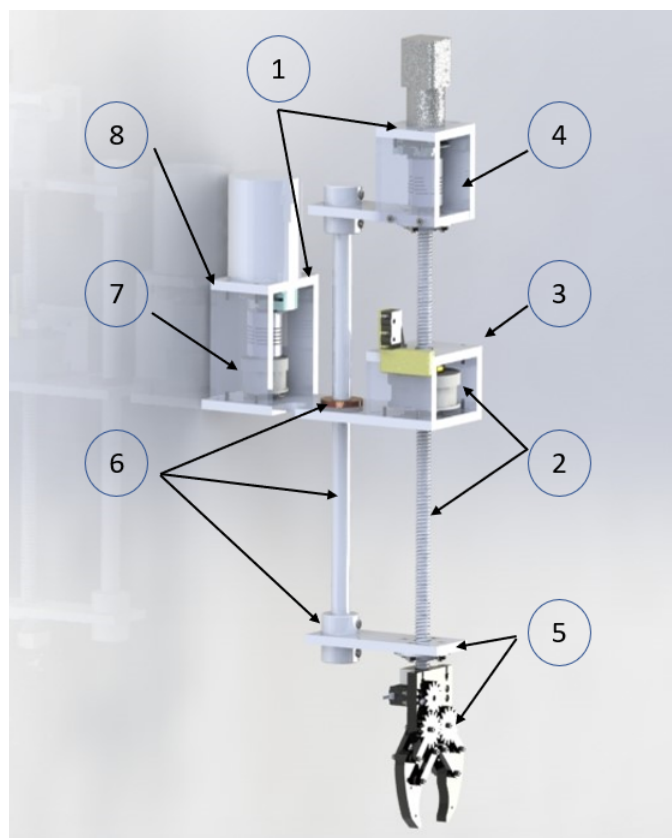


Figure 3.7: Assembly Steps

### 3.6 Final Assembly

After all the sub-assemblies are made, the electronics would be mounted within the base structure. The bearing housings for both the intermediate shafts and flanges assemblies would then be fixed

to the structure. The intermediate shaft could be assembled at the same time. Following this, the end effector would be assembled with the flanges assembly using M5 socket head cap screws. The sub assembly would be assembled to the base structure on the shoulder shaft. The belts and idlers for the transmission would be incorporated to the assembly here. Finally, the wiring and cover would be fitted, completing the assembly.

## 4 Testing Phase

The testing phase of the project was significantly impacted by Coronavirus, as described in Section 5.1. Testing of the robot would have been conducted in two distinct phases: Electronics Testing and Integrated Testing. Planned tests, completed and incomplete, are detailed in the following subsections.

### 4.1 Electronics Testing

#### 4.1.1 Component Verification Tests

Initially, tests were conducted to verify all components were functional. Future tests relying on several components and code may fail due to a faulty component, thus testing before integration could prevent delays in future testing.

- **Motor** - The motor was run (using mechatronics lab power supply) at 12 V, 24 V. It was later ran using the RS-125D Power Supply. Performed as expected.
- **Limit Switch** - Connected (COM) to 5 V source and (NC) to scope. NC returns high(1) on click and low(0) otherwise. Performed as expected.
- **Motor Driver** - ran a code to amplify PWM input from Arduino. Tested on oscilloscope and on motor. Performed as expected.
- **Encoder** - Attached it to motor and connected channels A, B and I to scope. A lead B on clockwise motion, and vice-versa. Channel I pulsed once for every 500 pulses of channel A/B. Performed as per expected.
- **Arduino Mega 2560** - Used to verify all other components. Since they performed as expected, it can be assumed that the Arduino is not faulty.

### 4.1.2 Sampling Frequency Test

This test investigates whether the AVR micro-controller can be used in place of several counters. To do this, the Arduino Mega 2560 R3, which contains an ATMega 2560 microcontroller, was used as the sample microcontroller. The maximum pulse frequency ( $f_p$ ) was calculated as per Eq. 4.1. Note that the CPR of channel A and B are 500, giving a total CPR ( $CPR_T$ ) of 1000.

$$f_p = \frac{\omega_0 \times CPR_T}{60} = \frac{2500 \times 1000}{60} \text{ Hz} = 41.66 \text{ kHz} \quad (4.1)$$

To test whether the Arduino could sample at Nyquist frequency ( $2 \times f_p$ ), the circuit shown in Fig. 4.1 was set up.

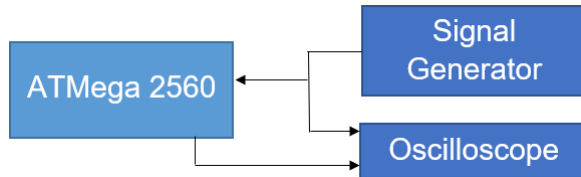


Figure 4.1: Sampling frequency test set-up

The signal generator would generate a pulse at a specific frequency and the Arduino was coded to replicate that signal. Although it managed to replicate the pulse from the signal generator on the oscilloscope at low frequencies, it started to miss pulses and (consequently) lag at higher frequencies, starting at around 30 kHz.

## 4.2 Integrated Testing

Due to the closure of the university campus before the end of the Spring term, the robot was not fully assembled. Mechanical testing of the prototype, therefore, could not be conducted. The tests that would have been used to validate the PDS requirements are described below:

### 4.2.1 Repeatability Testing

The PDS indicates that the robot arm must be able to return to a pre-defined location with less than  $\pm 0.1$  mm radial error. Measuring errors on this order of magnitude is difficult. Therefore a testing method was developed that aims to amplify the error for ease of measurement. The method involves fixing a powerful handheld laser to the end effector mechanism that shines onto a piece of paper which is fixed 100 m away. The position of the laser is recorded on the paper. The robot arm is programmed to move to an arbitrary position and return to the original position. The

difference between the two laser positions on the paper is measured and by scaling, the radial error of the robotic arm can be determined. This test should be performed twice, once by engaging the shoulder joint only and another by engaging the elbow joint only with the errors being added, thus returning the total error. Moreover, this test is more effective if performed at night where the laser is more observable.

#### 4.2.2 Linear Deviation Testing

This test is similar to the  $\pm 0.1$  mm repeatability test. A powerful handheld laser is fixed to the end effector mechanism which shines on to a piece of paper a fixed distance away. The laser position is marked on the paper. The arm is programmed to move by one encoder step and the new laser position is recorded on the paper. Accounting for the rotation of the shaft and the gear reduction ratio, the theoretical distance that the point should have travelled by can be determined. The actual deviation can be measured and compared against the theoretical deviation. By using scaling relations, the deviation at the end effector can be calculated. The test should be done once by engaging the shoulder shaft only and once by engaging the elbow shaft only. The total error will propagate thus the overall error may be determined.

#### 4.2.3 Maximum Speed and Acceleration Testing

The test for this criterion is simple and requires only the mechanical and electronic hardware as apparatus. The robotic arm is programmed to cover one stroke of the full working range. The encoder signals contain data regarding motor velocity, thus would be analysed to determine the maximum motor speed achieved. Utilising transmission ratios, the maximum joint speed may be determined. In addition, the time taken to attain maximum speed may be determined.

#### 4.2.4 Settling Time Testing

Set the robot to reach a specific location within the working envelope by engaging both the shoulder and elbow joint. Analyse the encoder signals to see if overshoot occurred and how long it took to reach steady state position. Repeat this test at multiple locations to verify that it is valid throughout the robot's working envelope.

### 4.2.5 End Effector Speed Testing

Calculate the amount of motor revolutions needed to cause the ACME lead screw to travel 150 mm and program the motor to do so. Using a slow motion feature on a smartphone camera, record the motion and analyse the footage to determine the time taken. Repeat this experiment for both directions to examine any effects due to gravity.

### 4.2.6 Mass and Storage Dimension Analysis

This two-part test is easy to implement but required the full assembly of the robot. To verify the mass of the robot place the SCARA robot on a large weighing scale. Check to see if the total weight is below that required in the PDS. Note that for the weight test, the power supplies should be excluded. Only the manufactured robot arm assembly should be included.

For storage dimension analysis, a testing rig may be constructed. A 30 x 30 x 30 cm cube structure may be constructed out of thin wooden beams. A contraction function may be written to the robot to get the robot limbs to fold as close to each other to minimise volume. The testing rig should then be placed over the robot to analyse storage dimensions.

## 5 Impact of Coronavirus

This design, make and test project was significantly impacted by the global outbreak of COVID-19. On 18<sup>th</sup> March 2020, an indefinitely long college-wide closure was announced, restricting access to manufacturing and testing facilities. Additionally, the Mechanical Engineering Department requested the submission of all hardware components of the project. The implications of the early shutdown on the progress of the project are detailed below.

### 5.1 Suspended Activities

As mentioned previously, the college closure due to the coronavirus outbreak created several unforeseen challenges in the development of the project. While the design phase of the project reached fruition, the manufacturing and testing phases were severely impacted. As per the original project timeline, manufacturing was due for completion at the end of spring term, with the time allocated purely to integrated system testing post-exams in the summer term. Given the progression of the pandemic, the following tasks remained incomplete:

### 5.1.1 End Effector Assembly

As most of the fixings were M2 screws and the M2 tapping set arrived just before the workshop was shut, the M2 internal threads could not be completed. Therefore assembly could not be completed although all of the purchased components have been delivered.

### 5.1.2 Full Assembly

As individual components of manufacturing were not complete, the full final product could not be assembled. The complete base structure, transmission elements, joints and flanges were completed and hence the robot was partially assembled before the early submission requested by the department. As previously stated, the manufacture of the end effector was not complete. Additionally, the integration and testing of the electronics to the mechanical hardware could not occur in the summer term as originally planned.

### 5.1.3 Control System Verification

To test the control system, the mechanical hardware was pivotal. While the system had been theoretically designed and component testing had been conducted, to verify the system integration testing was required. A dedicated three-week window had been allocated in the summer term specifically for this purpose. In-person testing and iterative development of the control algorithm could not take place.

## 5.2 Additional Work Package

To make up for the incomplete manufacturing and testing, each member of the team was assigned a supplementary work package to further investigate or model various aspects of the robot.

### 5.2.1 Reflected Inertial Calculations

Reflected inertia is the inertia that the motor 'feels' from the load that it is driving. Inertial ratio is an important parameter in robotics, which is defined as the ratio of the reflected inertia to the inertia of the motor itself. A value of 1:1 is ideal; anything above 10:1 is undesirable as unwanted transient behaviour (such as overshooting) is more likely to occur at these high values [30]. In short, the closer to a ratio of 1:1, the more accurate and responsive the system will be.

The reflected load is calculated by Eq. 5.1, where  $J_L$  is the inertia of the arm and the load it carries,  $N_T$  is the total reduction ratio due to gearing and  $J_G$  is the inertia of the gearbox.

$$J_R = \frac{J_L}{N_T^2} + J_G \quad (5.1)$$

For the robotic arm,  $J_L$  depends on the arm position. Therefore  $J_L$  is constantly changing during operation. As such, the maximum and minimum  $J_L$  was determined to define the range of inertia that the system experiences. The results of the inertial analysis are shown in Table 5.1:

Table 5.1: Results of inertial analysis

Parameter	Value
$N_T$	36
Motor Inertia	110 ( $gcm^2$ )
Max Shoulder Inertia	1934 ( $gcm^2$ )
Min Shoulder Inertia	683 ( $gcm^2$ )
Elbow Inertia	392 ( $gcm^2$ )
Max Shoulder Inertia Ratio	17.6
Min Shoulder Inertia Ratio	6.2
Elbow Inertia Ratio	3.6

The analysis assumed a transmission efficiency of 100%, total rigidity of the robot arm and negligible frictional forces. The maximum shoulder inertia ratio occurs at full extension with the 200 g payload. The maximum shoulder inertia ratio was 17.6. This was much higher than the recommended 10:1 ratio and therefore disruptive transient behaviour was likely when the robot is in operation. Several measures can be taken to counteract this problem. For each design change, there is a trade-off, as explained in Table 5.2.

Table 5.2: Methods of reducing  $J_R$  and trade-offs

Method	Reduction of $J_R$ and Trade-Off
Increase Reduction Ratio	According to Eq. 5.1, increasing the reduction ratio ( $N$ ) decreases the effect of $J_L$ and hence $J_R$ reduces as a result. Pulley size is increased and space wasted.
Use motor with greater inertia	Using a motor with greater inertia decreases the inertial ratio. Motors with greater inertia are generally bigger, heavier and consume more power
Make structure lighter	Mass of components decreases hence $J_L$ decreases. Lighter structures can compromise rigidity of the arm making it more 'wobbly'

### 5.2.2 Analytical Verification of Electronics

As per Eq. 4.1, the pulse frequency is 41.66 kHz. It was assumed that the motor reaches maximum speed during its operation. To verify this assumption, a calculation using Eq. 2.1 was carried out.

The elbow joint has the lowest moment of inertia, therefore experiences the greatest speeds.

Assuming no-load and the minimum elbow moment of inertia of  $392 \text{ gcm}^2$  ( see Section 5.2.1),

Fig. 5.1 shows the angular position and angular velocity progression with time. The robot's encoders show motor relative information. To accurately reflect the joint position and velocity the transmission ratio is used to scale the analysis.

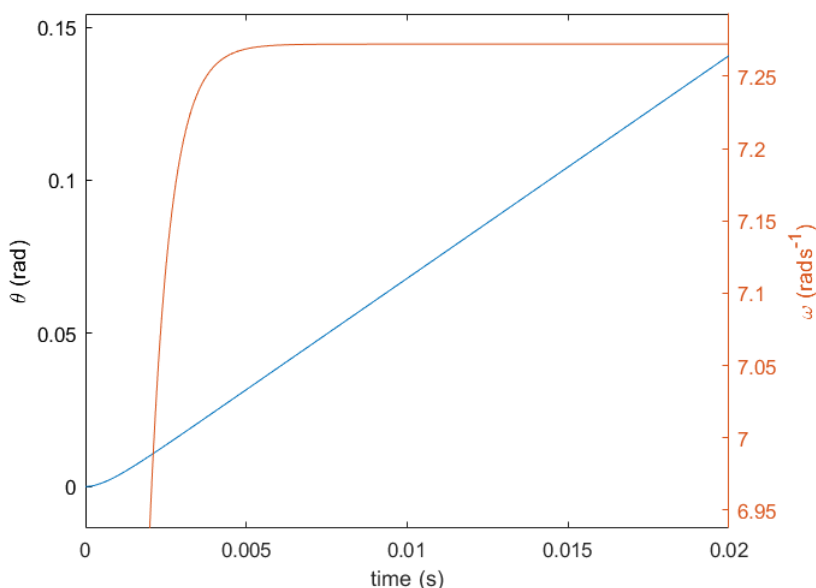


Figure 5.1: Angular Position and Angular Velocity vs Time for Elbow

As shown, the motor reaches maximum speed in 5 ms, verifying that for given loading conditions, the motor will reach max speed. This was expected as the motor was chosen to exceed requirements. The result also justifies the assumption of maximum speed in the pulse frequency calculation.

Due to the global pandemic, code could not be developed and tested. Therefore, the speed of the Arduino (the time it takes to execute the control algorithm) could not be tested. As an alternative, the execution time of common commands was determined using an online Arduino simulator on tinkercad. The `micros()` command returns the number of microseconds that pass since code has run. Two variables - `start` and `end` - were set equal to `micros()`. Then the command whose execution time was being measured was sandwiched between `start` and `end`. Finally, `end` minus `start` was printed.

As the `micros()` command has a resolution of  $8 \mu s$ , the commands were run sixteen times in between the start and end variables to get the execution time correct to  $0.5 \mu s$ . The final value (end minus start) was divided by sixteen to get the execution time of the command being tested. Table 5.3 shows the various commands that would be most likely used in the code, and their respective execution times .

Table 5.3: Execution time of common commands

Command	Execution time ( $\mu s$ )
Creating a variable	< 0.5
Storing a variable	1.5
Addition/Subtraction	< 0.5
<code>digitalRead</code>	6
Reading a data register (PIND for example)	2
<code>analogWrite</code>	16
<code>digitalWrite</code>	6

From Table 5.3, sampling of encoder signals using the Arduino required a minimum of  $19.5 \mu s$  (reading 3 encoder signals and storing a variable). The resulting sampling frequency is about 50 kHz (lower than Nyquist frequency of 80 kHz). Hence the sampling frequency was insufficient. Using the HCTL-2016, the position from the decoder can be read every  $7 \mu s$  (i.e. frequency at which it is reading position is approximately 143 kHz). This is done by exploiting the Arduino's ability to read a 8-bit register in  $2 \mu s$ . First, the lower 8 bytes are read ( $2 \mu s$ ) and stored ( $1.5 \mu s$ ). Then the upper 8 bytes are read and stored ( $3.5 \mu s$ ). To make this work, the SEL input (which controls which bits are being displayed on the counter) is connected to an external oscillator which switches every  $3.5 \mu s$ . This should theoretically yield a quicker response as positional feedback is obtained more often.

### 5.2.3 Control System Simulation in Simulink

The third component of the additional work package was modelling and simulation of the control loop for one axis of the robot. The purpose of the task was to test and tune the controller response in the absence of physical testing due to college closure. Although the full model was not developed due to time constraints and complexity of debugging issues, a large proportion of the control system was modelled numerically utilising the features of MATLAB and Simulink. This involved creating models at a component level. The modelling methodology is detailed below. The Simulink system is depicted in Fig. 5.2.

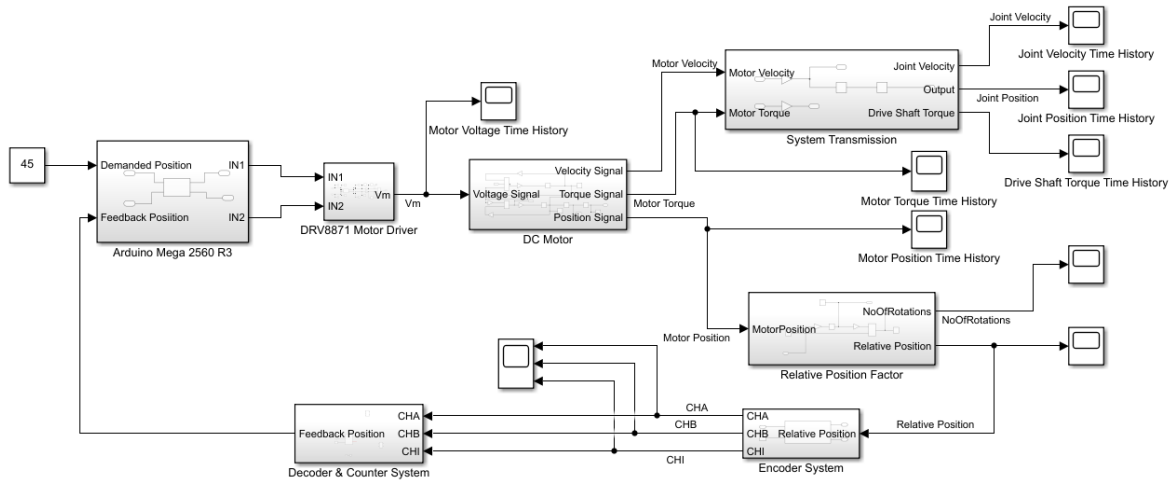


Figure 5.2: Control System in Simulink

The motor model was developed by extending the analysis taught in Machine System Dynamics [31]. A circuit diagram of the model is shown below in Fig. 5.3.

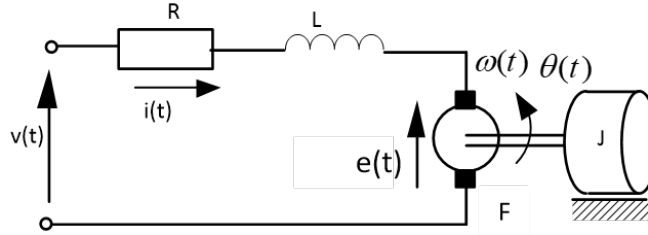


Figure 5.3: Circuit Diagram of DC Motor [31]

The motor was characterised by the transfer function in Eq 5.2, where  $v(t)$  is the applied voltage,  $R$  is the armature resistance,  $L$  is the armature inductance,  $e(t)$  is the generated back EMF,  $i(t)$  is the current,  $\omega(t)$  is the angular velocity,  $\theta(t)$  is the angular position,  $K_b$  is the motor constant,  $K_t$  is the torque constant,  $J$  is the rotor inertia and  $F$  is the motor viscous damping factor:

$$H(s) = \frac{\theta(s)}{v(s)} = \frac{K_t}{Ls^3 + (LF + RJ)s^2 + (RF + K_bK_t)s} \quad (5.2)$$

Using the transfer function block in Simulink and the appropriate coefficients, the motor model was defined. The motor driver was modelled using the truth table provided in the component datasheet (refer to Table 2.16).

From Table 2.16, two logic expressions that govern signals OUT1 and OUT2 were determined:

$$OUT1 = (\overline{IN2} \cdot IN1) + (\overline{IN2} \cdot \overline{IN1}) \quad (5.3)$$

$$OUT2 = (\overline{IN1} \cdot IN2) + (\overline{IN1} \cdot \overline{IN2}) \quad (5.4)$$

Using logic gate blocks in Simulink the gate circuit was constructed, as pictured in Fig. 5.4.

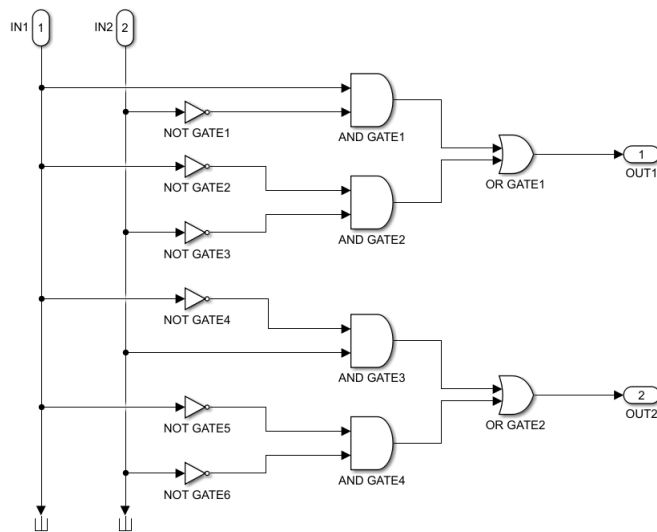


Figure 5.4: Gate Diagram of DRV8871 Motor Driver

The output signals were used to form a PWM signal that drives the H-bridge that controls the motor (refer to Fig. 2.26). To model the output voltage signals to the motor, the direction of rotation must be arbitrarily defined. In the developed model, high OUT1 drives the motor clockwise and high OUT2 drives the motor anticlockwise. Utilising the gain feature in Simulink, the output signals were modified and summed to produce an overall pulse, effectively simulating the motor driver component.

Developing a mathematical model of the encoder was initially challenging. However, a review of literature[32] indicated a method for describing the relationship between the shaft position and the encoder pulses. Fig. 5.5 depicts the operating mechanism of an optical encoder:

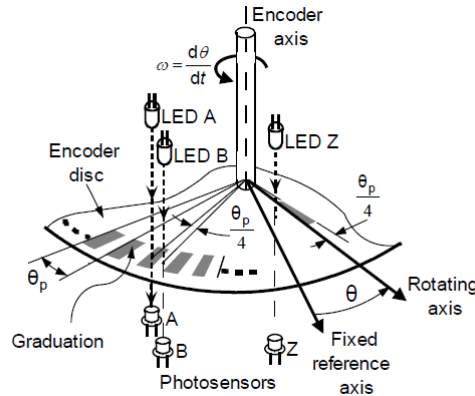


Figure 5.5: Operation Principle of Optical Encoder [32]

$\theta_p$  is defined as the graduation angle, which is physically interpreted as the angle between two consecutive code-wheel windows, which was calculated from Eq 5.5.

$$\theta_p = \frac{2\pi}{PPR} = \frac{18^\circ}{25} \quad (5.5)$$

Photosensors A and B are placed  $\frac{\theta_p}{4}$  apart, producing signals exactly out of phase. The signals were computed by a MATLAB function block in Simulink, taking the relative shaft position as an input and mathematically determining CHA, CHB and CHI signals. The mathematical functions of the signals are shown below in Eqs 5.6, 5.7 and 5.8.

$$A(\theta) = \begin{cases} 1 & 0 \leq \theta \pmod{\theta_p} \leq \frac{\theta_p}{2} \\ 0 & \frac{\theta_p}{2} \leq \theta \pmod{\theta_p} \leq \theta_p \end{cases} \quad (5.6)$$

$$B(\theta) = \begin{cases} 1 & 0 \leq \left(\theta - \frac{\theta_p}{4}\right) \pmod{\theta_p} \leq \frac{\theta_p}{2} \\ 0 & \frac{\theta_p}{2} \leq \left(\theta - \frac{\theta_p}{4}\right) \pmod{\theta_p} \leq \theta_p \end{cases} \quad (5.7)$$

$$I(\theta) = \begin{cases} 1 & \theta \pmod{360} = 0 \\ 0 & \theta \pmod{360} \neq 0 \end{cases} \quad (5.8)$$

Initially, the encoder model was inaccurately representing the CHA and CHB signals. Analysing the signals in the Simulink Data Inspector led to the conclusion that aliasing occurred due to inadequate sampling times. For the encoder to accurately contain direction and position information, the appropriate sampling frequency must be set. With the phase difference of the signals equal to a quarter of the graduation angle, information regarding state transition would be provided at this interval. Employing Shannon's sampling theorem, it was hypothesised that a step

size of  $\frac{\theta_p}{8}$  would solve the system aliasing. The appropriate frequency for sampling was determined using Eq 5.9 assuming a maximum velocity of 3000 RPM ( $100\pi$  rad/s).

$$f_s = \frac{1}{T} = \frac{100\pi}{\frac{\theta_p}{8} \frac{\pi}{180}} = \frac{144000}{\theta_p} = 200kHz \quad (5.9)$$

Once altering the sampling frequency, the issues regarding aliasing were rectified and more reliable signals for CHA and CHB were computed as shown in Fig 5.7.

The encoder data was passed to the decoder to extract the motor position. The principle for decoding was to count the number of clockwise ( $N_j$ ) and anti-clockwise pulses ( $N_i$ ), as was shown in Eq 2.8.

To decode the encoder pulses and find the direction of rotation, logic gate circuits are required. The circuitry required was not stated in the manufacturer datasheet or readily available in academic literature, thus logic network analysis methods were utilised. A quadrature decoder was modelled as a state machine, comparing the current state against the previous state to determine the values of Count Enable (1 if motion is detected, 0 if no motion) and Direction (1 if high and 0 is low). A third signal, Error, is also computed - the values of both A and B can not change in the same clock cycle, hence error signal is high in such an event. The finite state machine diagram is shown below in Fig 5.6 and the corresponding truth table is shown in Table 5.4.

Table 5.4: Quadrature Decoder Finite State Machine Table

Description	AB State		Outputs			
	Previous	Current	CommonEnable (CE)	Direction (D)	Error (E)	
Forward (A leads B)	00	10	1	1	0	
	10	11				
	11	01		0		
	01	00				
Backward (B leads A)	00	01	1	0	0	
	01	11				
	11	10		1		
	10	00				
No Motion	00	00	0	Previous Value of Direction when Common Enable was last high	1	
	01	01				
	10	10				
	11	11				
Error/Illegal Signals	00	11	0	1	1	
	01	10				
	10	01				
	11	00				

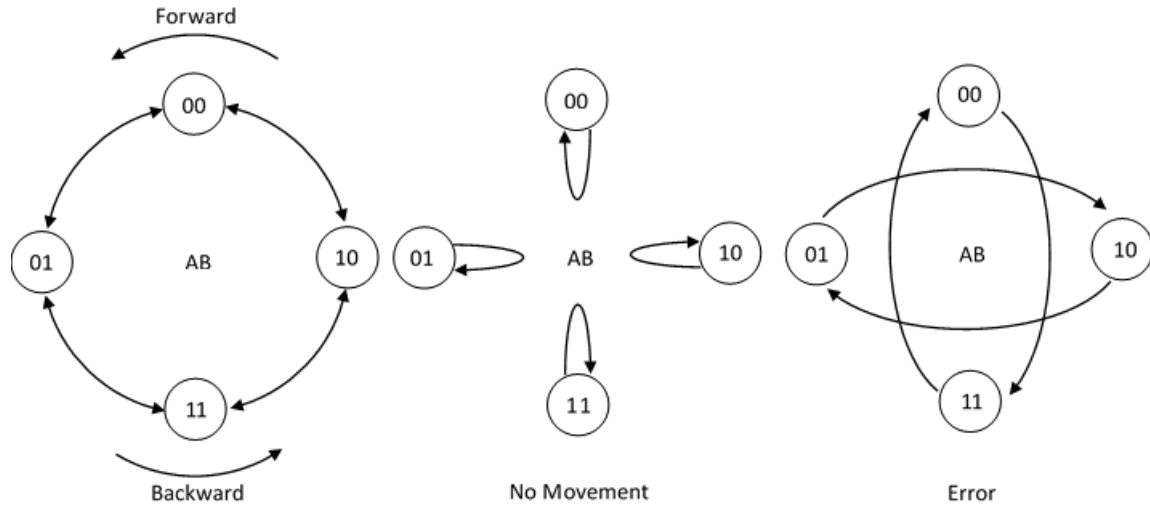


Figure 5.6: Quadrature Decoder Finite State Machine Diagram

From Table 5.4, Karnaugh maps were drawn for each output and the relevant boolean expressions derived:

$$\begin{aligned} CE = & \bar{A} \cdot B \cdot \bar{Q}_A \cdot \bar{Q}_B + A \cdot \bar{B} \cdot \bar{Q}_A \cdot Q_B + \bar{A} \cdot \bar{B} \cdot \bar{Q}_A \cdot Q_B + A \cdot B \cdot \bar{Q}_A \cdot Q_B \\ & + \bar{A} \cdot B \cdot Q_A \cdot Q_B + A \cdot \bar{B} \cdot Q_A \cdot Q_B + \bar{A} \cdot \bar{B} \cdot Q_A \cdot \bar{Q}_B + A \cdot B \cdot Q_A \cdot \bar{Q}_B \end{aligned} \quad (5.10)$$

$$D = A \cdot \bar{B} \cdot \bar{Q}_A \cdot \bar{Q}_B + \bar{A} \cdot \bar{B} \cdot \bar{Q}_A \cdot Q_B + \bar{A} \cdot B \cdot Q_A \cdot Q_B + A \cdot B \cdot Q_A \cdot \bar{Q}_B \quad (5.11)$$

$$E = A \cdot B \cdot \bar{Q}_A \cdot \bar{Q}_B + A \cdot \bar{B} \cdot \bar{Q}_A \cdot Q_B + \bar{A} \cdot B \cdot Q_A \cdot \bar{Q}_B + \bar{A} \cdot \bar{B} \cdot Q_A \cdot Q_B \quad (5.12)$$

From the boolean expressions, the logic circuits were designed in Simulink. The pulse generator function in Simulink was used to mimic motor driver signals. The integrated components were simulated. The results of the simulation are shown in Fig 5.7.

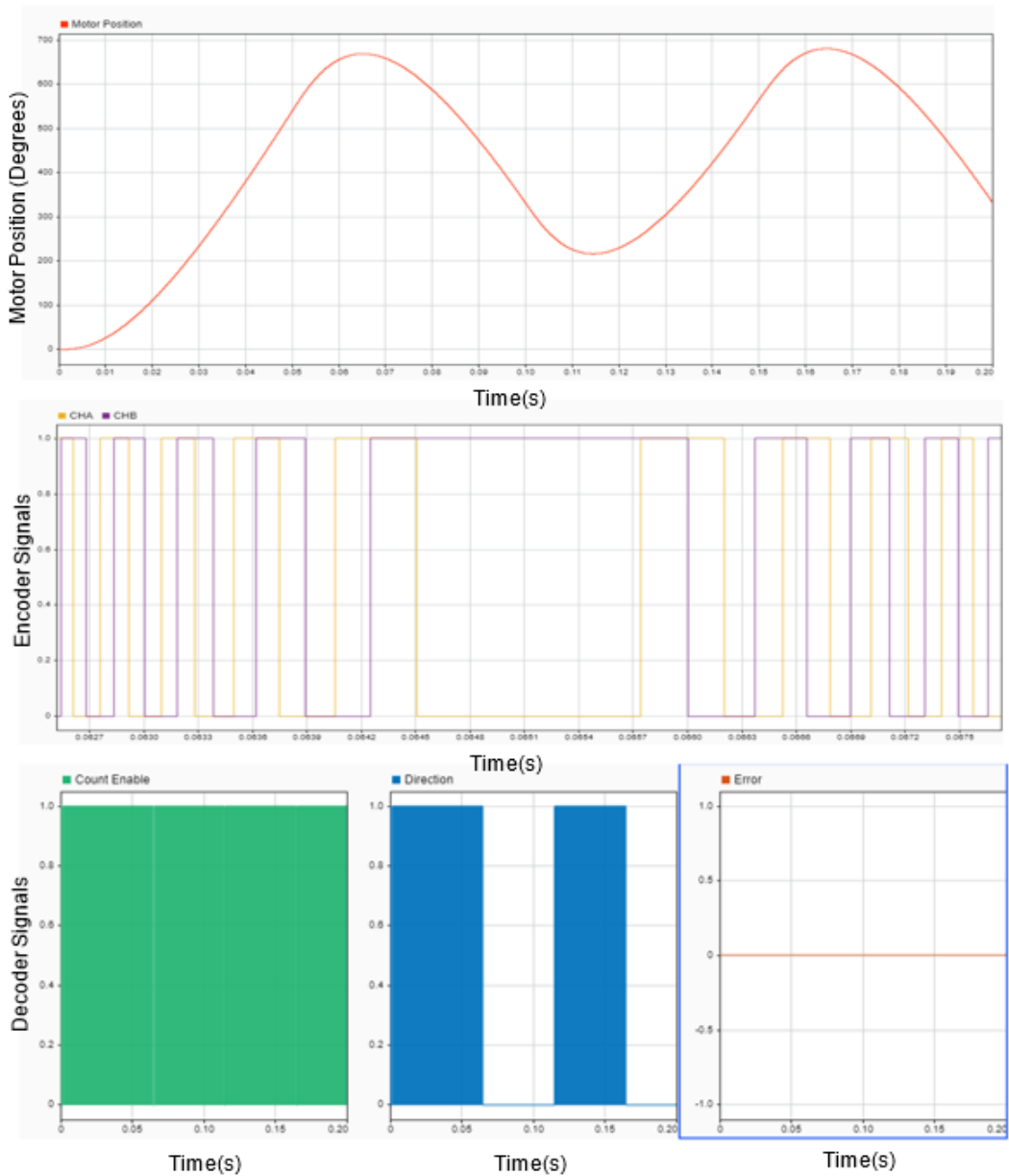


Figure 5.7: **Top:** Motor Position, **Middle:** Encoder Signals (zoomed in on change of direction), **Bottom:** Decoder Signals

The signals from the decoder and encoders are at high frequencies, hence each data point was not visible. However the data was analysed using Simulink Data Inspector. While the count enable and error signals shown in Fig 5.7 were as expected, the direction signal required further analysis. While the general form of the signal is as expected (high when driving forward, low when driving backward), the signal must be conditioned to enable an accurate position count. The direction signal oscillates between 1 and 0 when driving forward - instead the signal should stay high. The oscillation occurs due to the clock speed and state table. The high clock speed means that the sample time gives rise to the false presence of no motion states as the CHA and CHB will not have

changed between samples.

The HCTL-2016 has internal logic to smooth the signal which must be implemented in the Simulink model. However, due to the change in the control system triggered by the analysis detailed in Section 5.2.2, time constraints of the project and difficulties in debugging the decision was made to rest further work on simulation modelling. The position counter and control algorithm depicted in Fig 2.30 were yet to be implemented and can be considered as future work should the project be continued.

The maximum speed and acceleration of the robot were determined via simulation. These values were compared to stated criterion in the PDS, providing some product verification. By utilising the gain function blocks and transmission ratio the joint velocity, position and torque may be determined as shown in Fig 5.8.

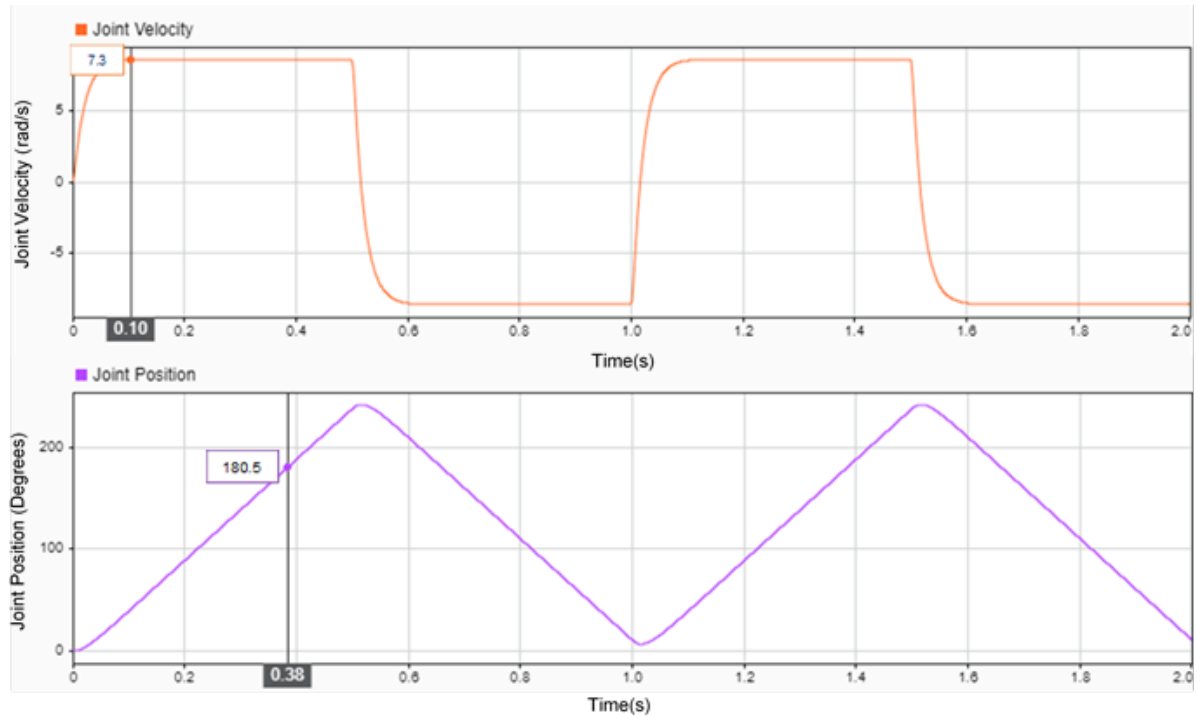


Figure 5.8: Simulation of Joint Motion

The maximum speed of the joints was determined as 7.3 rad/s, above the stated  $2\pi$  rad/s requirement. Additionally, the maximum speed was attained after 0.1 seconds. The PDS required max speed to be reached within 0.2 seconds, therefore the simulation provides verification for the acceleration criterion.

### 5.2.4 Motion Simulation with Simulink

Due to the impact of COVID-19, the final assembly was not finished. Therefore integrated testing was also not conducted. As an alternative, a virtual model of the robot was built using the Simscape Multibody™ add-in in Simulink [33] to simulate the motion of the product.

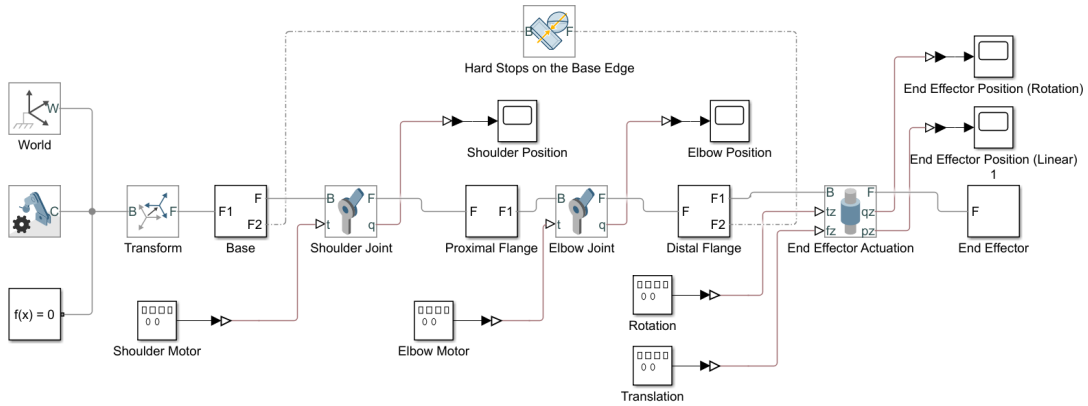


Figure 5.9: Simulink model of the robot

A simplified model was generated in the Simscape Multibody environment, as shown in Fig. 5.9. The estimated weight and moment of inertia calculated in Section 5.2.1 was applied to the simplified model, along with the virtual payload of 200 g. Four degrees of freedom, annotated with blue arrows in Fig. 5.10 were actuated and their position responses to the PWM signals are shown as the simulation results.

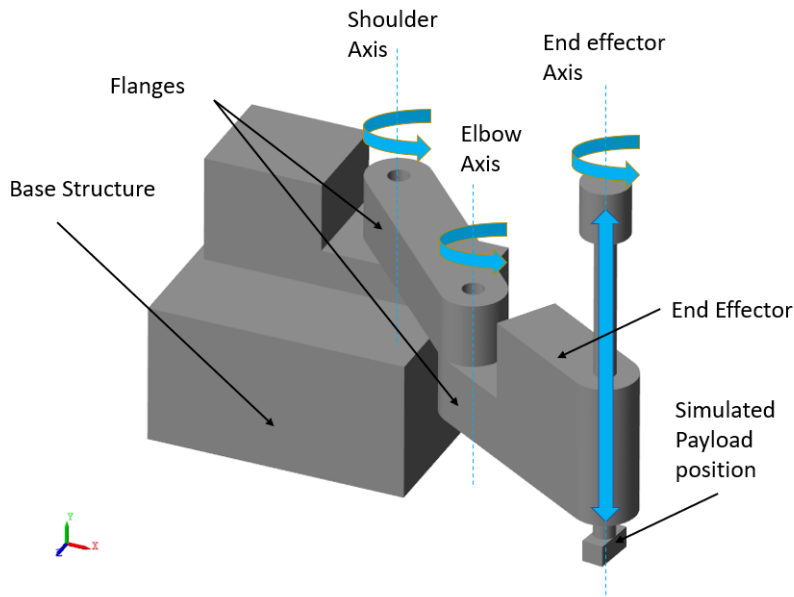


Figure 5.10: Simscape Multibody™ model of the robot

## 6 DISCUSSION AND CONCLUSION

---

The motion of each degree of freedom is shown in Fig. 5.11. It can be seen from the plots that both shoulder and elbow positions have small bounces at its limits. This is mainly the effects of the inertia of the flanges, end effector and the payload and could be reduced or eliminated by the introduction of the feedback control system.

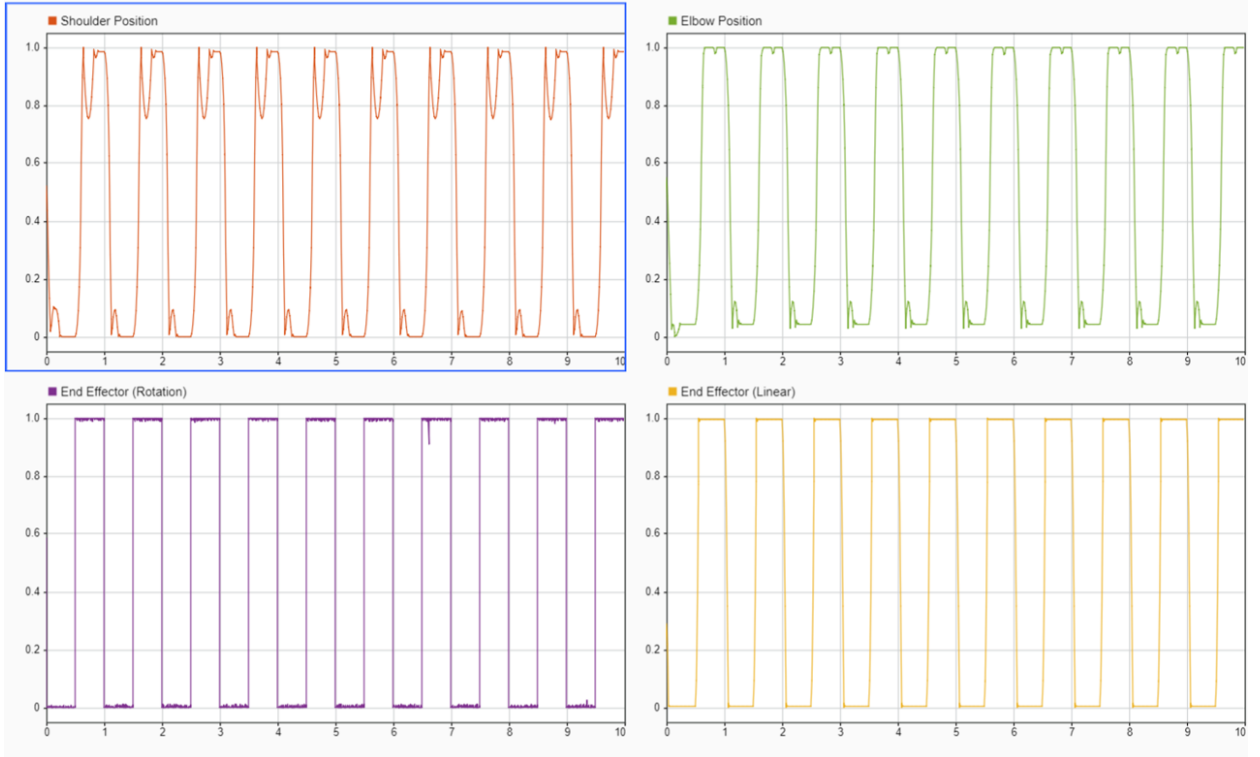


Figure 5.11: Four sensor results for four actuated degrees of freedom (normalised position against time (s))

The end effector degrees of freedom do not experience the same bounce as the shoulder and elbow. This was expected before simulation because the linear actuation is achieved by lead screws and should not have any bounces. The end effector rotational position has negligible bounces at its limits because the simulated payload has a small moment of inertia.

## 6 Discussion and Conclusion

### 6.1 Comparison to PDS

Table 6.1 details how the final product compares to the initial PDS requirements. Unfortunately, because of COVID-19, we were unable to fully assemble the robotic arm and hence a few of the key criterion could not be evaluated - these are marked in yellow. The successful objectives are marked in green and failed objectives are marked in red.

Table 6.1: Final Product Design Specification

Objective	Criteria	Verification
Weight	Total weight must be under 4 kg.	Total mass estimated in CAD as 12.9 kg
Size	Fit a 30 x 30 x 30 cm square space.	Measuring dimensions on CAD model indicates that final product would fit in a 35 x 35 x 30 cm <sup>3</sup> cube space
Payload Properties	Max payload of 200 g. Max dimensions: 10 cm x 5 cm x 2 cm. Min dimensions: 1 cm x 0.5 cm x 0.5 cm	The robot has been designed to support this weight. End Effector Gripper can handle the range of dimensions
Degrees of Freedom	Four Degrees of Freedom.	Robot has been designed from the beginning to operate in 4 DOF
Operating Angle	180 degrees	Arm's working envelope is 180 degrees according to CAD model
Operating Distance	Radius between 5 and 30 cm.	Working envelope ranges between 12.7 cm and 31.2 cm
Accuracy	Difference between actual and simulated positions $\pm 0.01$ mm linear deviation	Unable to perform test to validate this criteria
Repeatability	Less than $\pm 0.1$ mm error for repeated position	Unable to perform test to validate this criteria
Settling Time	Time taken for arm to stabilise after reaching intended position - 0.1 s max.	Unable to perform test to validate this criteria
Max Speed	At least $2\pi$ rad/s	Simulation verified that max angular velocity was 7.3 rad/s.
End effector speed	150mm vertical distance in at least 1.5 seconds	Unable to perform test to validate this criteria
Acceleration	Reach max angular velocity in less than 0.2 seconds.	Simulation verified that max angular velocity was reached in 0.1 seconds
Environment	Product expected to operate in indoor conditions 20-30 C°, no/low humidity. May be exposed to dust and debris (IP62). Critical transmission parts with IP65 (dustproof when storing).	The 3-D printed cover leaves no exposed transmission elements.
Product Life	Expected shelf life of 4/5 years.	All mechanical and electrical components satisfy this requirement
Service Life	3 hours of lab session every week, 35 weeks a year (315 hours total).	Mechanical components have been designed to withstand these operating hours
Repairability	Mechanical components must be easily replaceable.	Elbow joint difficult to disassemble due to dowel pins

Manufacturing	Easily reproducible.	Completely manufacturable with STW facilities and tools
Product Cost	Price per unit must be lower than competitor prices at the very least approximately £200 per unit.	Total cost of robot £455 with bulk buying discounts £640 without .
Safety	No sharp edges. No exposed transmission or electrical components.	The 3-D printed cover leaves no exposed transmission elements or sharp edges.
Disposal	Components (except motors/electronics) must be recyclable.	All components other than those stated are fully recyclable

The failed objectives must be discussed in further detail. Although the final assembly was never weighed, the CAD model estimates the mass as 12.9 kg. This is over the PDS requirement, but was expected given the amount of aluminium and steel used to assure high stiffness and heavy motors. Reflecting on this, we should have set a more realistic weight objective.

According to the CAD model, the smallest volume that our robot can occupy is  $35 \times 35 \times 30 \text{ cm}^3$ , thus the size criterion was not met. This was due to the body being bigger than anticipated because of the pulley sizes. Additionally, the height of the end effector mechanism was greater than anticipated. However the additional volume is minimal ( $0.00975 \text{ m}^3$ ), therefore the implications of failing this objective are minimal.

Due to the size of the base, the robotic arm has a minimum distance of 12.7 cm from the main axis (shoulder joint). The maximum range of the end effector was measured as 31.2 cm from the shoulder joint. This was due to slight adjustments during the design process (e.g elbow connectors) which pushed the distance above the desired 30 cm slightly. Due to the modular nature of the design, this error can be rectified easily by shortening one or both flanges.

For ease of maintenance, the robot arm must be easily disassembled. The design of the shoulder and elbow joint utilises dowel pins which are not easily removable. These were implemented for enhanced robot performance with the downside of failing this objective. Therefore the objective was viewed as a worthwhile sacrifice.

The final cost per unit of the robot was £455, after applying bulk buying discounts (£640 without). The cost price was over double the initially stated price in the PDS. However, when compared to the Arduino BRACCIO, the performance of the designed robot is superior in almost all aspects. Additional design work may be conducted to further reduce the cost price of the robot.

## 6.2 Proposal for Continuation

Should this project be taken up by a DMT group next year, there are a few key areas that can be further developed to enhance the performance, capability and educational potential of the robot. These are listed in Table 6.2.

Table 6.2: Proposal for Future Work

Evaluate Failed Objectives	Having evaluated and discussed the failed PDS objectives, the continuing team can either propose new designs that achieve the original objectives or redefine requirements.
Design Base Stand	Throughout the duration of the project, it was assumed that the robot would be mounted on a sturdy fixed stand that increases its vertical height for the end effector to have a full range of motion. For the robot to be functioning to its full potential, this stand must be designed.
Improve Range of Motion	A major difference between the FANUC and the designed robot is the range of motion. The product is limited to a 180° rotation and hence a smaller working envelope. Next year's team should investigate modifying the design to allow 360° rotation.
Investigate Software Elements of Robotic Design	Software is an important aspect of robotics. Investigating the software elements of robotics may lead to a more wholesome electromechanical design. One task would be to design a GUI for complex control such as path planning. Additionally, evaluating the requirements to utilise the features of ROS (Robotic Operating System) would allow for programming the robot to perform numerous tasks.
Investigate Simulation	Simulation is a powerful feature when designing robotics. The team should consider utilising Simulink and Simscape Multibody during the design phase to evaluate their choices before committing to a specific design. Existing models designed by the current team will be available as a starting point.
Implement Optical Vision	A true challenge would be to implement a camera system whereby the robot has vision capabilities and can track targets and execute movements accordingly. This would also add a 'computer vision' element to the lab which would even further enhance the educational experience.

## 6.3 Conclusion

The original proposal of this design, make and test project was to build a reproducible desktop robot, suitable for robotics teaching in the upcoming 'Introduction to Robotics' module. The project brief stated that the product should have at least four degrees of freedom. It was also stated that robot accuracy and mechanical characteristics (high stiffness/low backlash) should be maximised.

Maximisation was an ambiguous goal, however, the team decided to make the project an engineering challenge and rival industry-standard robots. The robot's performance requirements were based on the £30500 FANUC SR-3iA industrial robot. With the high standards demanded, the restricted budget, limited time and lack of robotics knowledge the project was always going to be a monumental task. Despite the challenges, however, the team persevered, dedicating hours to researching, iterating and building a superior robotic arm to the BRACCIO for an objectively marginal increase in price.

Due to COVID-19, the team were unable to fully test our robot to evaluate performance against the FANUC's. Therefore the key parameters were not quantitatively established. Some estimates were developed through simulation and analysis. The maximum joint speed was found to be 7.3 rad/s. The system accelerated to max speed within 0.1 seconds, providing a very fast and powerful robot. The majority of PDS requirements (See Fig. 6.1) were verified despite the early college shut down. The product failed to meet a few of them; most important being the operating distance criteria, total mass and the final cost of the robot.

Overall, complete technical evaluation of the project was difficult given the halt due to COVID-19. Assuming the worst-case scenario of failing all untested criteria, the DMT was still a successful learning experience that produced a much more capable, useful and impressive robot than the BRACCIO, despite the final product costing almost 3 times as much. By setting the bar high and aiming for industry-standard performance, while simultaneously incorporating an educational aspect to our robot, the team developed a strong appreciation of principles of engineering design. The project provided the students with a strong foundation to continue delving into the field of robotics while developing important technical and soft skills to apply to future projects.

## 7 Personal Reflective Reviews

### 7.1 Kyriacos Theocharides

Building a robotic arm with specifications of a £30 000 industrial machine for a retail price of £200 to teach university undergraduate students the fundamentals of robotics is about as ambitious and challenging as engineering projects come. However, I feel that setting almost impossible standards and valiantly working towards them was a fantastic educational experience that pushed us to previously untouched boundaries and realms of knowledge.

As project manager, I was responsible for calling team meetings, keeping track of the team's progress and constantly evaluating the direction in which the project was heading, as well as

designing and manufacturing the flanges and elbow joint while also conducting motor and transmission research in the project's early stages. While I am overall satisfied with my engineering contribution, there were a few aspects of my team management work which could have been better executed.

Firstly, I feel that I was somewhat disorganised as a project manager as I was often unsure of exact deadlines and what was specifically required for them. A good project manager doesn't need to know everything about the project (this is an impossible feat), but should by all means be 'on top' of tasks and have a clear vision of the direction of the project; something which I certainly could have done better.

Secondly, I failed to clarify exactly what was being asked for right at the beginning of the project. For example, I spent hours researching servo and stepper motors for the joints only to be informed that these were not suitable for teaching control as you cannot build control loops for them. Had I clarified such requirements earlier, we would have saved a lot more time by not chasing dead ends.

Thirdly, I didn't efficiently allocate tasks and track the individual team member's progress in the first term. This did improve after I implemented Dr. Ristic's suggestion of switching from a general team Gantt chart to a 'personal' Gantt chart, where individual weekly targets were set rather than general team targets. Had this method been implemented right from the beginning, I believe we would have been a lot more productive.

Overall, I learnt that success in team projects stems from clarity in communication and complete understanding of the problem at hand and what needs to be done. Despite not achieving a few of our original objectives, I'm still very happy with what we accomplished and feel that lofty and ambitious targets actually enhanced our learning experience rather than diminishing it.

I would like to thank Dr. Ristic for his constant help and advice and for encouraging us to set our expectations high and work towards them. I would also like to thank my teammates for their hard work, self sacrifice and dedication. Lastly, I would like to thank the STW personnel (notable mentions Aslan and Paul) for their guidance and patience.

## 7.2 Aman Didwania

The DMT has been the biggest project undertaking of my life so far. It entailed various stages such as planning, concept design and review, manufacture and testing. Each stage has been very educational and enriching, and has taught me several essential hard and soft skills.

Firstly, I'd like to thank our supervisor, Dr. Ristic. He would always set high targets for us and push

us to go further. He was easily approachable and gave a lot of guidance and feedback on our work.

The project was to build a robot for next year's ME4 Introduction to Robotics module. The fact that our work could leave a visible mark on Imperial over the next few years was a huge motivator. Within the first month of working on the project, it felt like the whole team was emotionally attached to the project.

After selecting motors and deciding on the robot structure, the team split into 2 units - Mechanical and Electrical. I was part of the electrical unit. Due to the nature of the work, I was often required to apply the concepts I was being taught in ME3 Modules such as Machine System Dynamics and Embedded C in Micro-controllers; giving me a deeper appreciation and understanding of the material being taught. This is especially true for signal measurement and processing; while testing, I ran into several problems related to hardware being unable to measure signals from the encoder which forced me to look into alternate ways of measurement and transmission of encoder data. It is a shame that manufacture and testing couldn't be completed due to covid-19, but I definitely feel satisfied with the work that I have put in and moreover, the knowledge and understanding I have achieved.

My other role on the team was the inventory and budget manager. I was responsible for the ordering and arrival of components/material. I feel like I was able to experience having a 'bird's eye view' on everything as I had to look at not only my own work but the work of the manufacturing team (i.e. who needed what and when did they need it by) as well. Given the high demands of the project and low budget, I had to often search for cheaper substitutes (Motor, Encoders, Pulleys, Belts, Aluminium, etc.) which did not compromise on performance (or compromised performance within reason). I feel that this skill of searching for substitute components will definitely help me later on in my engineering career.

As a final note, I'd like to thank my teammates. Everyone was very friendly and encouraging, pardoning and making up for each others mistakes. If the virus clears out and time permits in ME4, I'd like to try and finish what we started together.

### 7.3 Jinhong Wang

As the largest project in college so far, the experience of DMT has been very educational, teaching me how to approach a brand-new project and complete the tasks progressively.

Since this project is quite stand-alone and without previous work, understanding the project is crucial for the following development. At the early stage of the project, a lot of time was spent on

literature research and the design specifications. Then, getting into the design phase, the team was naturally split into mechanical and electronic design teams. Quite a few iterations for motor selection and mechanical design were gone through to make sure that the final design is reasonable and easily manufacturable. Approaching the end of the design phase, manufacturing started from the sub-assemblies that are already finalised, giving a smooth transition into the next stage of the project. Unfortunately, due to the impact of COVID-19, although the manufacturing was coming along the plan, it could not be finished and the rest of the project (testing) has to be done remotely by simulations.

In general, the project is progressing well with the plan. Although more time was spent as expected at the design phase, the slack in the Gantt chart was used and the improved design really saved us a lot of time in manufacturing. The additional work package also suits to the project well and would help in the future follow-up for this project.

I was in charge of the mechanical designing and CAD during the design phase. I went through all the design iterations and produced engineering drawings for most of the components, which helped me improve my CAD skills. In addition, I had to coordinate with other teammates for the components ordering, budget considerations, and assembly of CAD for different sub-assemblies. Getting into manufacturing, I had to consult different people in the department for design suggestions and manufacturing tips. It was challenging to me because I was always afraid to talk to people. However, I am glad that I was finally able to overcome my fear and stepped out of my comfort zone. I also learned how to use Simulink Simscape Multibody when completing the additional working package.

For the next project, I would try to improve my communication skills further. In addition, in both ME2 and ME3 projects, I was doing mechanical design and CAD so I would like to experience other roles next time such as team manager.

To sum all, although we were not able to complete the project as expected at the beginning of the year, we still learned a lot of stuff throughout the project and gained meaningful experiences that would help in the future.

## 7.4 Advaith Sastry

The opportunity to develop a low cost, high-accuracy robotic manipulator for our DMT project was an invaluable experience. With a personal interest in control engineering and robotics, I wanted to develop important professional and transferable skills, and it was rewarding to find my teammates had the same passion and drive to succeed. Working alongside my team and our

supervisor, Dr Ristic, has been an incredible experience.

Defining product specifications took longer than expected - while this is typically an iterative process in a client-orientated environment, this stage was extended too long and affected the flow of the project. This used most of the slack afforded in the project timeline, leaving little room for error as the project progressed. In future projects, defining objectives at an earlier stage will be beneficial. The rest of the project was conducted efficiently, making up for the lost time. Although incomplete due to the onset of COVID-19, the experience of undertaking a major engineering project was not diminished.

I was involved in many aspects of the project. As the project developed there was a natural division of tasks: Electrical and Mechanical design. I assisted in the selection of electronics components and the design of the control system. Verifying the system led to proficiency in analysing component datasheets, a valuable skill for any engineer. Additionally, I was responsible for developing the GUI for the end-user, allowing me to investigate the software engineering aspects of the project and expand my multidisciplinary appreciation. I authored documentation for the system electronics: designing schematics and learning the intricacies of EagleCAD. Finally, I developed a large portion of the Simulink model of the control system to assist in the absence of on-site testing. In doing so, I developed an appreciation of numerical modelling and simulation.

I was also the data and documentation manager for the project. I took responsibility for organising the information generated throughout the project. I had oversight on project reporting, thus taking point on structuring/reviewing submissions and other materials. I also performed quality control on documentation to ensure produced material was of the highest standard. This role gave me an appreciation for the importance of communication of technical information.

In addition to technical and soft skills, I learned an important lesson regarding time management. My module selection for ME3 meant I had a very coursework intensive year, with a large consistent workload throughout the year. This meant at times my focus was drawn away from DMT, reducing my availability and slowing the flow of the project. In future projects, I will work on prioritising tasks to ensure avoidable delays are minimised. DMT has provided an incredible basis for personal and professional development. The importance of communication within the team and effective organisation to meet project deadlines shines through as some of the key takeaways. I have thoroughly enjoyed the experience and look forward to what I have learnt in the future.

## 7.5 Yikai Wang

DMT is the largest project that I have done so far, given a very raw concept to start with and finally assembling and making it work with excellent quality has been very challenging but also satisfying. Although COVID-19 has impacted the completion of the project, it has been very educational and meaningful, nonetheless.

At the start of the project, after discussion and brainstorming, each of us has been allocated a task. My role was responsible the end effector, which is a crucial component for the whole project, from designing to manufacturing at the highest standard possible and kept within a reasonable budget.

It seemed like an impossible task at the beginning as I had no idea how and where to start because there were so many factors that needed to be taken into consideration, from how the mechanisms works to material and motor selection. After many hours of researching of existing examples and understanding the mechanism, I presented ideas that seemed viable to my team members. After countless discussions and iterations to improve the design with the support of my team and supervisor, the idea was decided eventually. Draft CAD models of different ideas was made allowing visual representation which aided the selection of the concepts. Motor and pulley calculations were subsequently carried out which took many hours as there were countless options and factors that needed to be taken into consideration. It has been challenging deciding the optimal combination of motor and pulley due to the space available on the plate, budget available and power available. After these have been decided, I re-examined the design and made alterations according to the selection and presented the updated concept to my team and supervisor which was finally approved and ready to be manufactured. Engineering drawings were produced accordingly and orders for rest of the components were placed. Manufacturing of the end effector was then carried out according to the Gantt chart.

Looking back on the project, despite the end effector being complicated and challenging, I was satisfied with the progress I have made but there are also areas I need to improve.

During the designing phase of the end effector, I was often late on deadline. On one hand it was due to the workload I had from LRP and ECM which occupied a lot of time but more importantly I realised I could've planned and managed my time better. I now understand the importance to meet deadline otherwise the project would be infinitely delayed, and the work produced might not be as detailed and thought through.

Throughout each phase of the project, I feel like I haven't communicated enough with my team members on my progress and the help I need. Sometimes when a problem arises, I just carry on

with my own and end up not solving it or taking much more time than needed. In the future projects, I will work more on communication with my team members as a clear communication improves the efficiency overall.

## References

- [1] Wikipedia contributors, *Scara — Wikipedia, the free encyclopedia*, <https://en.wikipedia.org/w/index.php?title=SCARA&oldid=945130242>, [Online; accessed 22-May-2020].
- [2] *Scara robots, fanuc*, <https://www.fanuc.eu/tr/en/robots/robot-filter-page/scara-series/selection-support>, [Online; accessed 25-May-2020].
- [3] Wikipedia contributor, *Articulated robot — Wikipedia, the free encyclopedia*, [https://en.wikipedia.org/w/index.php?title=Articulated\\_robot&oldid=948377201](https://en.wikipedia.org/w/index.php?title=Articulated_robot&oldid=948377201), [Online; accessed 22-May-2020].
- [4] *Tinkerkit braccio robot, arduino*, <https://store.arduino.cc/tinkerkit-braccio-robot>, [Online; accessed 25-May-2020].
- [5] A. Elfasakhany, E. Yanez, K. Baylon, R. Salgado, et al., "Design and development of a competitive low-cost robot arm with four degrees of freedom," *Modern Mechanical Engineering*, vol. 1, no. 02, p. 47, 2011, [Online; accessed 24-May-2020].
- [6] S. P. Kadrimangalam Jahnavi, "Teaching and learning robotic arm model," *International Conference on Intelligent Computing, Instrumentation and Control Technologies (ICICICT)*, 2017, [Online; accessed 24-May-2020].
- [7] Wikipedia contributors, *Cartesian coordinate robot — Wikipedia, the free encyclopedia*, [https://en.wikipedia.org/w/index.php?title=Cartesian\\_coordinate\\_robot&oldid=935663633](https://en.wikipedia.org/w/index.php?title=Cartesian_coordinate_robot&oldid=935663633), [Online; accessed 22-May-2020].
- [8] *Gantry 3 axis, robot gantry*, <https://robotgantry.com/gantry-robot-3-axis/>, [Online; accessed 25-May-2020].
- [9] A. Klimchik, "Enhanced stiffness modeling of serial and parallel manipulators for robotic-based processing of high performance materials," PhD thesis, 2011.
- [10] Wikipedia contributor, *Serial manipulator — Wikipedia, the free encyclopedia*, [https://en.wikipedia.org/w/index.php?title=Serial\\_manipulator&oldid=912798848](https://en.wikipedia.org/w/index.php?title=Serial_manipulator&oldid=912798848), [Online; accessed 22-May-2020].
- [11] F. Lijin and S. Longfei, "Design of a novel robotic arm with non-backlash driving for friction stir welding process," *The International Journal of Advanced Manufacturing Technology*, vol. 93, no. 5-8, pp. 1637–1650, 2017.
- [12] *Fanuc sr-3ia*, <https://www.fanuc.eu/tr/en/robots/robot-filter-page/scara-series/scara-sr-3ia>, [Online; accessed 27-May-2020].
- [13] R. Budynas and K. Nisbett, *Shigley's Mechanical Engineering Design*. McGraw-Hill Education, 2014, ISBN: 9780073398204.
- [14] *Dmn37 motors, nidec servo corporation*, [http://www.nidec-servo.com/en/digital/pdf/DMN37\\_1.pdf](http://www.nidec-servo.com/en/digital/pdf/DMN37_1.pdf), [Online; accessed 24-May-2020].
- [15] Uxcell, *30rpm 12ga 6v 3mm shaft mini dc geared gear box motor for robot*, <http://www.uxcell.com/30rpm-12ga-3mm-shaft-mini-geared-gear-box-motor-for-robot-p-441765.html>, [Online; accessed 22-May-2020].
- [16] *Acme and lead screw assembly glossary and technical data, nook industries, inc*, <https://www.nookindustries.com/acme/AcmeGlossary.cfm>, [Online; accessed 25-May-2020], Nov. 2019.

- [17] *Types of robots based on configuration*, <https://www.plantautomation-technology.com/articles/types-of-robots-based-on-configuration>, [Online; accessed 24-May-2020].
- [18] P. R. Childs, *Chapter 4 - Machine Elements*, P. R. Childs, Ed. Oxford: Butterworth-Heinemann, 2014, pp. 121–137, ISBN: 978-0-08-097759-1. DOI: <https://doi.org/10.1016/B978-0-08-097759-1.00004-6>. [Online]. Available: <http://www.sciencedirect.com/science/article/pii/B9780080977591000046>.
- [19] C. D. Bellicoso, L. R. Buonocore, V. Lippiello, and B. Siciliano, “Design, modeling and control of a 5-dof light-weight robot arm for aerial manipulation,” in *2015 23rd Mediterranean Conference on Control and Automation (MED)*, IEEE, 2015, pp. 853–858.
- [20] Servocity, *Standard gripper kit a*, <https://www.servocity.com/standard-gripper-kit-a>, [Online; accessed 05-June-2020].
- [21] *Aedb-9140 series datasheet*, <http://www.farnell.com/datasheets/2343281.pdf>, [Online; accessed 27-May-2020].
- [22] *Hctl-2032 conversion to the hctl-2016 and hctl-2020 avago technologies*, <https://docs.broadcom.com/doc/5989-2699EN>, [Online; accessed 23-May-2020].
- [23] *Quadrature decoder/counter interface ics datasheet*, *avago technologies*, <https://www.ascl.ece.vt.edu/docs/HCTL2000.pdf>, [Online; accessed 22-May-2020].
- [24] *Crystal clock oscillator specifications, iqd frequency products*, <https://www.iqdfrequencyproducts.com/products/details/cfps-73-14-01.pdf>, [Online; accessed 21-May-2020].
- [25] J. Dimitrov, “Memory and i/o strategies. serial and parallel comms,” *De Montfort University Leicester*, [Online; accessed 27-May-2020].
- [26] *Drv8871 3.6-a brushed dc motor driver with internal current sense (pwm control)*, *texas instruments*, <https://cdn-shop.adafruit.com/product-files/3190/dr8871.pdf>, [Online; accessed 27-May-2020].
- [27] *Aedb-9140 series three channel optical incremental encoder modules with codewheel, 100 cpr to 500 cpr*, *broadcom*, <https://docs.rs-online.com/34ce/0900766b812cdcb0.pdf>, [Online; accessed 24-May-2020].
- [28] *125w triple output switching power supply datasheet, mean well*, <https://docs.rs-online.com/a04b/0900766b8136feb2.pdf>, [Online; accessed 25-May-2020].
- [29] B. S. Institute, *Bs 4235-1:1972*, Feb. 1972.
- [30] B. Knight, *Understanding inertia ratio and its effect on machine performance*, *mitsubishi electric*, <https://www.engineeringwhitepapers.com/motion-control/understanding-inertia-ratio-and-its-effect-on-machine-performance/>, [Online; accessed 20-May-2020].
- [31] M. Ristic, “Machine system dynamics: Part 1 control systems,” *Imperial College London*, 2019.
- [32] I. I. Incze, A. Negrea, M. Imecs, and C. Szabó, “Incremental encoder based position and speed identification: Modeling and simulation,” *Acta Univ Sapientiae Electr Mech Eng*, vol. 2, pp. 27–39, 2010.
- [33] *Simscape multibody*, *mathworks*, <https://www.mathworks.com/products/simmechanics.html>, [Online; accessed 20-May-2020].